molecular pharmaceutics

Article

New flavone-cyanoacetamide hybrids with combination of cholinergic, antioxidant, modulation #-amyloid aggregation and neuroprotection properties as innovative multifunctional therapeutic candidates for Alzheimer's disease and unraveling their mechanism of action with acetylcholinesterase

Shaik Jeelan Basha, Penumala Mohan, Daniel Pushparaju Yeggoni, Zinka Raveendra Babu, Palaka Bhagath Kumar, Ampasala Dinakara Rao, Rajagopal Subramanyam, and Amooru Gangaiah Damu

Mol. Pharmaceutics, **Just Accepted Manuscript** • DOI: 10.1021/acs.molpharmaceut.8b00041 • Publication Date (Web): 10 May 2018

ACS Publications

is published by the American Chemical Society. 1155 Sixteenth Street N.W., Washington, DC 20036

New flavone-cyanoacetamide hybrids with combination of cholinergic, antioxidant, modulation β-amyloid aggregation and neuroprotection properties as innovative multifunctional therapeutic candidates for Alzheimer's disease and unraveling their mechanism of action with acetylcholinesterase

Shaik Jeelan Basha[a], *Penumala Mohan*[a], *Daniel Pushparaju Yeggoni*[b], *Zinka Raveendra Babu*[a], *Palaka Bhagath Kumar*[c], *Ampasala Dinakara Rao*[c], *Rajagopal Subramanyam*[b], *Amooru Gangaiah Damu*[a,]*

[a]Department of Chemistry, Yogi Vemana University, Andhrapradesh, Kadapa, India

[b]Department of Plant Sciences, School of Life Sciences, University of Hyderabad, Hyderabad, India

[c]Centre for Bioinformatics, School of life Sciences, Pondicherry Central University, Puducherry, India

*Corresponding author

Prof. Amooru Gangaiah Damu

Department of Chemistry

Yogi Vemana University

Andhrapradesh-Kadapa-516003 India

Tel: +91-9177888961

Email: agdamu01@gmail.com

KEYWORDS: Alzheimer's disease, flavones, cyanoacetamide, Multi-target Directed Ligands, binding studies, circular dichroism spectroscopy, fluorescence emission, molecular docking.

ABSTRACT

In line with the modern multi target-directed ligand paradigm of Alzheimer's disease (AD), a series of nineteen compounds composed of flavone and cyanoacetamide groups have been synthesized and evaluated as multifunctional agents against AD. Biological evaluation demonstrated that compounds **7j**, **7n**, **7o**, **7r** and **7s** exhibited excellent inhibitory potency (AChE, IC_{50} 0.271 ± 0.012 to 1.006 ± 0.075 μM) and good selectivity toward acetylcholinesterase, significant antioxidant activity, good modulation effects on self-induced Aβ aggregation, low cytotoxicity and neuroprotection in human neuroblastoma SK-N-SH cells. Further, an inclusive study on the interaction of **7j**, **7n**, **7o**, **7r** and **7s** with AChE at physiological pH 7.2 using fluorescence, circular dichroism and molecular docking methods suggesting that these derivatives bind strongly to peripheral anionic site of AChE mostly through hydrophobic interactions. Overall, the multifunctional profiles and strong AChE binding affinity highlight these compounds as promising prototypes for further pursuit of innovative multifunctional drugs for AD.

INTRODUCTION

Alzheimer's disease (AD) is a progressive neurodegenerative disease that assaults the central nervous system (CNS) leading to memory loss, cognitive impairment, behavioral disturbances and loss of intellectual ability[1]. With more than 48 million people afflicted worldwide,[2] AD has become one of the biggest global public health challenges.[3] As a result of increasing incidence, progressive clinical onset, mortality and unavailability of definitive treatments, AD has a severe impact on patients' and their families' quality of life and its economic burden is massive.[4] Although the etiology of AD remain elusive, substantial evidences have revealed that AD is a multifactorial syndrome derived from a complex array of neurochemical factors, such as low levels of synaptic acetylcholine (ACh), oxidative stress and accumulation of neurotoxic amyloid beta peptide, dyshomeostasis of biometals, the inflammation of neurons, and so on. Several hypotheses based on these factors have been proposed to explain the mechanism of AD pathogenesis.[5, 6]

Based on the ''cholinergic hypothesis'', AChE and BuChE inhibition have been documented as critical targets for the effective management of AD by an increase the availability of ACh in the brain regions.[7] However, recently it has been reported that serious inhibition of BuChE also may contribute to peripheral side effects.[8] The tacrine a dual AChE and BuChE inhibitor, which showed serious hepatotoxicity as well as other side effects was withdrawn from the market.[9] Therefore, the potential advantage of selective inhibition of AChE over BuChE may include lesser degree of associated side effects. So it may be a good approach to expand selective AChE inhibitors for the treatment of AD, with expectation for their fewer unfavorable effects.[3]

According to "amyloid hypothesis", the production and accumulation of oligomeric aggregates of amyloid-β (Aβ) peptide in the brain are a central event in the pathogenesis of AD.[10] Among

the main isoforms, $A\beta_{42}$ is a major component of the amyloid plaques and plays a critical role in the initiation of plaque formation and AD pathogenesis.[11] The most toxic forms of Aβ including senile plaques, fibrils, protofibrils, and oligomers are among the aggregates of amyloidogenic peptides.

However, it has been reported that among the toxic amyloidogenic peptides including oligomers protofibrils, fibrils, and senile plaques, oligomers are more toxic to neurons in comparison with the fibril aggregates.[12] It has also been reported that synaptic loss in the cerebral cortex is related to the concentration of soluble Aβ monomers and oligomers.[13, 14] In support for this, a variety of molecules have been designed to modulate the aggregation of amyloidogenic peptides.[15] Therefore, finding molecules that ubiquitously modulate biological effects of the aggregates of amyloidogenic peptides is a complementary approach and a matter of active research.

A wealth of experimental data shows that the reactive oxygen species (ROS) is another major etiological factor of AD since amyloid plaques and neurofibrillary tangles along with ROS overproduction are the main factors for the initiation of neuroinflammation that precede neuronal degeneration in AD patients.[16] Consequently, neuroprotection against oxidative damage in neuronal cells has become highly beneficial and worthy strategy for either the prevention or the treatment of AD.[17]

Therefore, the combination of selective AChE inhibition, Aβ aggregation modulation, reduction of oxidative load and neuroprotection represents an additional rational approach for AD management. Facing the complex etiology of AD, at present researchers are focused on developing new Multi-target Directed Ligands (MTLDs) to fight back against this disease.[18, 19] In this context, by exploiting MTDL approach, several hybrid molecules, which consist of two or

more pharmacophores in one molecule and could simultaneously target different pathogenic factors of AD have been reported as successful multifunctional agents to treat AD.[20]

Our group is also actively engaged to develop potent MTLDs against AD and recently reported tricyclic coumarin analogs as hybrids of coumarin and cyanoacetamides as potential multifunctional anti-AD.[21, 22] Herein; we have developed a novel series of flavone derivatives to investigate their multifunctional potential against AD. Flavones have been assessed for several therapeutic activities against AD like AChE inhibitory,[23] neuroprotective, antioxidant, Aβ fibril formation inhibitory, reduction effect of H_2O_2-induced ROS formation and GSK tau aggregation inhibitory activities.[24] On the other hand the cyanoacetamide scaffold is widely used to develop numerous biologically active agents.[25, 26]

To proceed with our goal, flavone moiety was selected to combine with cyanoacetamide fragment as well as variety of amides into single frame, to design a series of flavones derivatives **7a**–**s**, to test their multifunctional activities. In this paper, a series of nineteen derivatives were designed, synthesized and evaluated biological activities including AChE and BuChE inhibition, the kinetics of enzyme inhibition, anti-oxidative effects, neuroprotective effects against H_2O_2-induced SKSNH cell injury, amyloid-β peptide (Aβ) modulating abilities based on the multitarget-directed ligands strategy (MTDLs). Further, we have used both biophysical and computational approach to understand the binding mechanism of target compounds with AChE.

MATERIALS AND METHODS

Analytical grade starting materials and reagents were purchased from commercial sources (Aldrich, Merck) and were used without purification. Prior the use, all the solvents were purified

and dried by standard methods. Progress of the reactions were monitored using analytical thin-layer chromatography (TLC) on silica gel 60 F_{254} plates with a layer thickness of 0-20 mm from sigma (USA), and visualized with an UV lamp (254 nm). Column chromatography was performed on silica gel (Merck, 200-400 mm mesh or less than 200 mm). Melting points were determined in open capillary tubes on a Fisher Scientific apparatus (India) and were uncorrected. IR spectra were measured as KBr discs with a Perkin Elmer Spectrum two spectrophotometer (Singapore) and reported the frequency of absorption (cm^{-1}) in the range from 4000 to 400 cm^{-1}. ^{1}H NMR (400 MHz) and ^{13}C NMR (100 MHz) were recorded at room temperature in $CDCl_3$ solution using Bruker Avance II (Switzerland) spectrometer. NMR spectra of representative compounds are shown in the Supplementary Information. Chemical shifts are reported in parts per million (δ ppm) relative to tetramethylsilane (TMS), an internal standard. The peak multiplicity was indicated by abbreviations viz.: s = singlet; d = doublet; t = triplet; q = quartet; m = multiplet; bs = broad singlet. Mass spectra were obtained on an Agilent LC/MSD trap SL 1100 series mass spectrometer with a 70 eV (ESI probe) in positive mode and high-resolution mass spectra were obtained by using ESI-QTOF mass spectrometry in positive mode.

Preparation of resacetophenone (1)

Freshly fused 33 g of $ZnCl_2$ was dissolved in 32mL of acetic acid while heating; 22 g of resorcinol was added. The reaction mixture was heated to 140-150^{0}C and stirred for 15 min. After being settled for 1h, the mixture was treated with 100 mL of 1:1 HCl to break the zinc chloride complex. The reaction was cooled to 5^{0}C and the resulted solid was filtered. The product was further crystallized from 20% HCl to get 90% yield of compound **1**.[27,28]

Preparation of 1-(4-benzoyloxy-2-hydroxyphenyl)-3-phenyl-1,3-propanedione (2)

To a mixture of resacetophenone **1** (4.56 g, 30 mmol) and powdered potassium carbonate (30.36 g, 220 mmol) in 150 mL of anhydrous acetone, benzoyl chloride (7 mL, 60 mmol) was added drop wise with stirring at room temperature. The resulting mixture was refluxed for 20 h. After being cooled to room temperature, the deposits were filtrated off. The filtrate then poured into 530 mL of 10% glacial acetic acid and formed yellow solid was collected by filtration and recrystallized from acetone to give 51 % yield of desired product **2**. [29, 30]

Preparation of 7-hydroxyflavone (3)

A mixture of 100 mL of concentrated sulphuric acid and compound **2** was stirred for 4 h keeping the temperature of the reaction mixture not beyond 5 °C. The liquid was poured into 500 g of ice under vigorous stirring to give a white solid, which was filtered, washed thoroughly with water and dried. To this solid, 250 mL of 5% potassium carbonate solution was added. The mixture was heated to 100 °C and stirred for 1 h. To the reaction mixture was acidified with concentrated hydrochloric acid by adding drop wise to pH = 5 and white solid thus formed was collected by filtration. After drying, the raw material was recrystallized from absolute ethanol to give 82 % yield of 7-hydroxyflavone.[31]

Preparation of 8-formyl-7-hydroxyflavone (4)

Under microwave irradiation at 300 W for 7 min, hexamethylenetetramine (HMTA) (5.6 g, 40 mmol) was added to a solution of 7-hydroxyflavone (2.52 g, 10 mmol) in glacial acetic acid (50 mL). The reaction mixture was treated with 20% HCl (50mL) and further irradiated for another 4 min with MW at 200 W. After cooling to room temperature, the reaction solution was poured

into crushed ice. The acidic solution was extracted with ether (500 mL × 1, 250 mL × 2). The combined organic phases were washed three times with 10% sodium bicarbonate solution (100 mL ×3), dried over Na_2SO_4 and filtered. The solvent was evaporated to dryness under reduced pressure to get the pale yellow solid. The afforded solid was recrystallized from ethanol to get 75% yield of compound **4**.[32]

General procedure for the preparation of cyanoacetamides 6(a-s)

To a solution of ethylcyanoacetate **5** (1.2 mmol) in ethanol (10 mL), the appropriate amine (1 mmol) was added in an easily available screw cap bottle. The mixture was stirred at room temperature for 5-8 h and monitored by TLC. Once the reaction had completed, the reminder was cooled down to 0-5 °C in an ice bath. In most cases, the obtained amide, typically precipitated after some minutes to hours.[21, 22] The deposit was filtered off and washed several times with ether to obtain pure N-substituted cyanoacetamide derivatives.

General synthetic procedure for preparation of final products 7(a-s)

To a solution of compound **4** (1.5 mmol) and appropriate N-substituted cyanoacetamide (**6a-s)** (3.1 mmol) in ethanol (10 mL), was added Et_3N (0.1 mmol) drop wise at room temperature. The resulting mixture was refluxed for 2-3 h. After that, the reaction mixture was allowed to cool to room temperature. The precipitated product was collected by filtration and washed with cold methanol (2-3 mL) to yield corresponding final products (**7a-s)**.[33]

8-imino-N-methyl-4-oxo-2-phenyl-4H,8H-pyrano[2,3-f]chromene-9-carboxamide (7a)

Off white solid; yield 67%; mp: 213–215°C; IR (KBr) ν_{max}: 3436, 3239, 3068, 2925, 2854, 1730, 1677, 1643, 1606, 1555, 1437, 1351, 1199, 1078, 827, 774, 686 cm^{-1}; ^1H NMR (400 MHz, $CDCl_3$) δ: 10.02 (br s, 1H, 12-NH), 9.05 (s, 1H,10-H), 8.28 (d, 1H, *J* = 8.8 Hz, 5-H), 7.95 (d, 2H, *J* = 6.0 Hz , 2'-H and 6'-H), 7.81 (s, 1H, 8-NH), 7.55 (m, 3H, 3'-H, 4'-H and 5'-H), 7.16 (d, 1H, *J* = 8.8 Hz, 6-H), 6.85 (s, 1H, 3-H), 3.01 (d, 3H, *J* = 4.4 Hz, 1''-CH_3); ^{13}C NMR (100 MHz, $CDCl_3$) δ: 176.9 (C-4), 163.6 (C-2), 162.3 (C-6a), 157.2 (C-8), 156.4 (C-11), 153.2 (C-1a), 134.2 (C-1'), 132.2 (C-10), 131.0 (C-4'), 129.8 (C-5), 129.5 (C-3', 5'), 126.4 (C-2', 6'), 121.0 (C-4a), 120.0 (C-9), 113.4 (C-10a), 109.2 (C-6), 108.2 (C-3), 26.6 (C-1''); ESI-MS *m/z*: 347.4 $[M+H]^+$; HRMS calcd. For $C_{20}H_{15}O_4N_2$: 347.3876, found: 347.3885.

N-ethyl-8-imino-4-oxo-2-phenyl-4H,8H-pyrano[2,3-f]chromene-9-carboxamide (7b)

Off white solid; yield 68%; mp: 176–178°C; IR (KBr) ν_{max}: 3442, 3252, 3075, 2972, 2922, 1680, 1645, 1587, 1556, 1436, 1383, 1352, 1198, 1031, 830, 771, 685 cm^{-1}; ^1H NMR (400 MHz, $CDCl_3$) δ: 10.10 (br s, 1H, 12-NH), 9.06 (s, 1H, 10-H), 8.28 (d, 1H, *J* = 8.8 Hz, 5-H), 7.95 (m, 2H, 2'-H and 6'-H), 7.81 (s, 1H, 8-NH), 7.55 (m, 3H, 3'-H, 4'-H and 5'-H), 7.16 (d, 1H, *J* = 8.8 Hz, 6-H), 6.85 (s, 1H, 3-H), 3.49 (m, 2H, 1''-CH_2), 1.27 (t, 3H, *J* = 7.6 Hz, 2''-CH_3) ; ^{13}C NMR (100 MHz, $CDCl_3$) δ: 176.9 (C-4), 163.6 (C-2), 161.5 (C-6a), 157.2 (C-8), 156.4 (C-11), 153.2 (C-1a), 134.2 (C-1'), 132.2 (C-10), 131.0 (C-4'), 129.8 (C-5), 129.4 (C-3', 5'), 126.4 (C-2', 6'), 121.1 (C-4a), 120.0 (C-9), 113.4 (C-10a), 109.2 (C-6), 108.2 (C-3), 34.9 (C-1''), 14.7 (C-2''); ESI-MS *m/z*: 361.4 $[M+H]^+$; HRMS calcd. For $C_{21}H_{17}O_4N_2$: 361.3786, found: 361.3791.

N-dodecyl-8-imino-4-oxo-2-phenyl-4H,8H-pyrano[2,3-f]chromene-9-carboxamide (7c*)*

Off white solid; yield 67%; mp: 115–117°C; IR (KBr) ν_{max}: 3447, 3318, 3223, 3064, 2921, 2850, 1729, 1680, 1651, 1624, 1559, 1543, 1438, 1384, 1353, 1199, 1077, 827, 774, 686 cm^{-1}; ^1H NMR (400 MHz, $CDCl_3$) δ: 10.12 (br s, 1H, 12-NH), 9.03 (s, 1H, 10-H), 8.26 (d, 1H, *J* = 8.8 Hz, 5-H), 7.94 (d, *J* = 6.4 Hz, 2H, 2'-H and 6'-H), 7.81 (s, 1H, 8-NH), 7.54 (m, 3H, 3'-H, 4-H' and 5'-H), 7.15 (d, 1H, *J* = 8.8 Hz, 6-H), 6.84 (s, 1H, 3-H), 3.43 (m, 2H, 1"-CH_2), 1.62 (m, 2H, 2"-CH_2), 1.37 (br s, 18H, 3"–11"-CH_2), 0.85 (t, 3H, *J*= 6.4 Hz, 12"-CH_3); ^{13}C NMR (100 MHz, $CDCl_3$) δ: 176.9 (C-4), 163.5 (C-2), 161.5 (C-6a), 157.1 (C-8), 156.4 (C-11), 153.2 (C-1a), 134.2 (C-1'), 132.2 (C-10), 131.0 (C-4'), 129.7 (C-5), 129.4 (C-3', 5'), 126.4 (C-2', 6'), 121.0 (C-4a), 120.0 (C-9), 113.3 (C-10a), 109.2 (C-6), 108.1 (C-3), 40.1 (C-1"), 32.0 (C-2"), 29.7 (C-3"), 29.7 (C-4"), 29.6 (C-5"), 29.4 (C-6",7"), 29.4 (C-8",9"), 27.2 (C-10"), 22.7 (C-11"), 14.2 (C-12"); ESI-MS *m/z*: 510.3 $[M+H]^+$; HRMS calcd. For $C_{31}H_{37}O_4N_2$: 510.7753, found: 510.7761.

N-cyclopropyl-8-imino-4-oxo-2-phenyl-4H,8H-pyrano[2,3-f]chromene-9-carboxamide (7d)

Off white solid; yield 75%; mp: 204–206°C; IR (KBr) ν_{max}: 3437, 3250, 3065, 2925, 2853, 1730, 1670, 1646, 1606, 1580, 1480, 1350, 1199, 1075, 830, 775, 687 cm^{-1}; ^1H NMR (400 MHz, $CDCl_3$) δ: 10.13 (br s, 1H, 12-NH), 9.06 (s, 1H, 10-H), 8.27 (d, 1H, *J* = 8.8 Hz, 5-H), 7.95 (d, 2H, *J* = 6.4 Hz, 2'-H and 6'-H), 7.77 (s, 1H, 8-NH), 7.54 (m, 3H, 3'-H, 4'-H and 5'-H), 7.15 (d, 1H, *J* = 8.8 Hz, 6-H), 6.85 (s, 1H, 3-H), 2.95 (m, 1H, 1"-H), 0.86 (m, 2H, 2"-CH_2), 0.64 (m, 2H, 3"-CH_2); ^{13}C NMR (100 MHz, $CDCl_3$) δ: 176.9 (C-4), 163.5 (C-2), 163.0 (C-6a), 157.1 (C-8), 156.3 (C-11), 153.2 (C-1a), 134.2 (C-1'), 132.2 (C-10), 131.0 (C-4'), 129.8 (C-5), 129.4 (C-3', 5'), 126.3 (C-2', 6'), 120.8 (C-4a), 120.0 (C-9), 113.3 (C-10a), 109.2 (C-6), 108.1 (C-3), 23.0 (C-1"), 6.58 (C-2", 3"); ESI-MS *m/z*: 373.5 $[M+H]^+$; HRMS calcd. For $C_{22}H_{17}O_4N_2$: 374.0125, found: 374.0069.

N-cyclohexyl-8-imino-4-oxo-2-phenyl-4H,8H-pyrano[2,3-f]chromene-9-carboxamide (7e)

Off white solid; yield 71%; mp: 190–192°C; IR (KBr) ν_{max}: 3437, 3240, 3066, 2924, 2853, 1728, 1676, 1648, 1620, 1585, 1542, 1437, 1385, 1352, 1195, 1067, 828, 775, 687 cm^{-1}; ^1H NMR (400 MHz, $CDCl_3$) δ: 10.12 (d, 1H, *J* = 7.2 Hz, 12-NH), 9.04 (s, 1H, 10-H), 8.26 (d, 1H, *J* = 8.8 Hz, 5-H), 7.94 (d, 2H, *J* = 6.4 Hz, 2'-H and 6'-H), 7.81 (s, 1H, 8-NH), 7.54 (m, 3H, 3'-H, 4'-H and 5'-H), 7.15 (d, 1H, *J* = 8.8 Hz, 6-H), 6.84 (s, 1H, 3-H), 3.97 (m, 1H, 1''-H), 1.97 (m, 2H, 2'-CH_2), 1.73 (m, 2H, 6'-CH_2), 1.61-1.27 (m, 6H, 3',4',5'-CH_2); ^{13}C NMR (100 MHz, $CDCl_3$) δ: 176.9 (C-4), 163.5 (C-2), 160.5 (C-6a), 157.1 (C-8), 156.3 (C-11), 153.1 (C-1a), 134.1 (C-1'), 132.2 (C-10), 131.0 (C-4'), 129.7 (C-5), 129.4 (C-3', 5'), 126.3 (C-2', 6'), 121.2 (C-4a), 120.0 (C-9), 113.3 (C-10a), 109.2 (C-6), 108.1 (C-3), 48.8 (C-1''), 32.6 (C-2'',6''), 25.7 (C-4''), 24.6 (C-3'',5''); ESI-MS *m/z*: 415.6 $[M+H]^+$; HRMS calcd. For $C_{24}H_{21}O_4N_2$: 415.6650, found: 415. 6704.

8-imino-2-phenyl-9-(pyrrolidine-1-carbonyl)pyrano[2,3-f]chromen-4(8H)-one (7f)

Off white solid; yield 65%; mp: 210–212°C; IR (KBr) ν_{max}: 3436, 3228, 3064, 2925, 2885, 1739, 1646, 1631, 1431, 1385, 1191, 1066, 775, 685 cm^{-1}; ^1H NMR (400 MHz, $CDCl_3$) δ: 8.40 (d, 1H, *J* = 8.8 Hz, 5-H), 7.88 (m, 3H, 10-H, 2'-H and 6'-H), 7.83 (s, 1H, 8-NH), 7.56 (m, 3H, 3'-H, 4'-H and 5'-H), 7.15 (d, 1H, *J* = 8.8 Hz, 6-H), 6.82 (s, 1H, 3-H), 3.68 (m, 2H, 2''-CH_2), 3.53 (m, 2H, 5''-CH_2) 1.95 (m, 4H, 3''-H and 4''-H); ^{13}C NMR (100 MHz, $CDCl_3$) δ: 177.2 (C-4), 164.0 (C-2), 163.4 (C-6a), 157.1 (C-8), 156.9 (C-11), 152.6 (C-1a), 134.2 (C-1'), 132.1 (C-10), 131.3 (C-4a), 129.4 (C-3', 5'), 128.5 (C-4'), 126.6 (C-5), 126.3 (C-2', 6'), 119.8 (C-9), 113.8 (C-10a), 109.2 (C-6), 108.3 (C-3), 46.1(C-2'', 5''), 24.4 (C-3'', 4''); ESI-MS *m/z*: 387.5 $[M+H]^+$; HRMS calcd. For $C_{23}H_{19}O_4N_2$: 387.6650, found: 387. 6704.

8-imino-2-phenyl-9-(piperidine-1-carbonyl)-4H,8H-pyrano[2,3-f]chromen-4-one (7g)

Off white solid; yield 71%; mp: 210–212°C; IR (KBr) ν_{max}: 3454, 3228, 3064, 2937, 2885, 1732, 1640, 1592, 1431, 1385, 1194, 1067, 861, 776, 685 cm^{-1}; ^1H NMR (400 MHz, $CDCl_3$) δ: 8.21 (d, 1H, *J* = 8.8 Hz, 5-H), 7.88 (m, 2H, 2'-H and 6'-H), 7.83 (s, 1H, 10-H), 7.56 (m, 3H, 3'-H, 4'-H and 5'-H), 7.40 (s, 1H, 8-NH), 7.15 (d, 1H, *J* = 8.8 Hz, 6-H), 6.81 (s, 1H, 3-H), 3.74 (br s, 2H, 2"-CH_2), 3.40 (br s, 2H, 6"-CH_2) 1.70 (br s, 6H, 3"-H, 4"-H and 5"-H); ^{13}C NMR (100 MHz, $CDCl_3$) δ: 177.0 (C-4), 164.1 (C-2), 163.4 (C-6a), 157.2 (C-8), 156.9 (C-11), 152.5 (C-1a), 134.2 (C-1'), 132.2 (C-10), 131.3 (C-4a), 129.4 (C-3', 5'), 128.5 (C-4'), 126.5 (C-5), 126.3 (C-2', 6'), 119.8 (C-9), 113.8 (C-10a), 108.6 (C-6), 108.2 (C-3), 47.3 (C-2", 6"), 25.5 (C-3", 5"), 24.4 (C-4") ; ESI-MS *m/z*: 401.6 $[M+H]^+$; HRMS calcd. For $C_{24}H_{21}O_4N_2$: 401.6120, found: 401. 6151.

8-imino-9-(morpholine-4-carbonyl)-2-phenyl-4H,8H-pyrano[2,3-f]chromen-4-one (7h)

Off white solid; yield 68%; mp: 218–220°C; IR (KBr) ν_{max}: 3445, 3220, 3064, 2981, 2924, 2856, 1651, 1593, 1484, 1470, 1448, 1388, 1355, 1252, 1218, 1194, 1068, 1111, 987, 776, 683 cm^{-1}; ^1H NMR (400 MHz, $CDCl_3$) δ: 8.24 (d, 1H, *J* = 8.8 Hz, 5-H), 7.89 (m, 3H, 10-H, 2'-H and 6'-H), 7.81 (s, 1H, 8-NH), 7.58 (m, 3H, 3'-H, 4'-H and 5'-H), 7.15 (d, 1H, *J* = 8.8 Hz, 6-H), 6.83 (s, 1H, 3-H), 3.81 (br s, 4H, 3"-H and 5"-H), 3.72 (m, 4H, 2"-H and 6"-H); ^{13}C NMR (100 MHz, $CDCl_3$) δ: 176.9 (C-4), 164.4 (C-2), 163.4 (C-6a), 157.1 (C-8), 156.9 (C-11), 152.6 (C-1a), 134.2 (C-1'), 132.2 (C-10), 131.3 (C-4a), 129.4 (C-3', 5'), 128.9 (C-4'), 127.8 (C-5), 126.3 (C-2', 6'), 119.9 (C-9), 113.8 (C-10a), 108.5 (C-6), 108.3 (C-3), 66.7 (C-3", 5"), 47.3 (C-2", 6"); ESI-MS *m/z*: 403.5 $[M+H]^+$; HRMS calcd. For $C_{23}H_{19}O_5N_2$: 404.0220, found: 404. 0251.

N-benzyl-8-imino-4-oxo-2-phenyl-4H,8H-pyrano[2,3-f]chromene-9-carboxamide (7i)

Off white solid; yield 80%; mp: 220–222°C; IR (KBr) ν_{max}: 3448, 3305, 2925, 1730, 1675, 1650, 1620, 1587, 1548, 1438, 1386, 1353, 1190, 1066, 848, 775, 687 cm^{-1}; ^1H NMR (400 MHz, $CDCl_3$) δ: 10.56 (br s, 1H, 12-NH), 9.08 (s, 1H, 10-H), 8.28 (d, 1H, *J* = 8.8 Hz, 5-H), 7.94 (m, 2H, 2'-H and 6'-H), 7.81 (s, 1H, 8-NH), 7.55 (m, 3H, 3'-H, 4-H' and 5'-H), 7.36 (m, 5H, 2''-H, 3''-H, 4''-H, 5''-H and 6''-H), 7.15 (d, 1H, *J* = 8.8 Hz, 6-H), 6.84 (s, 1H, 3-H), 4.67 (d, 2H, *J* = 5.6 Hz, 13-H); ^{13}C NMR (100 MHz, $CDCl_3$) δ: 176.8 (C-4), 163.6 (C-2), 161.7 (C-6a), 157.2 (C-8), 156.2 (C-11), 153.2 (C-1a), 138.2 (C- 1''), 134.5 (C-1'), 132.2 (C-10), 131.0 (C-4'), 129.9 (C-5), 129.4 (C-3', 5'), 128.8 (C-3'', 5''), 127.6 (C-2'', 6''), 127.4 (C- 4''), 126.4 (C-2', 6'), 120.9 (C-4a), 120.1 (C-9), 113.4 (C-10a), 109.2 (C-6), 108.2 (C-3), 44.0 (C-13); ESI-MS *m/z*: 423.2 $[M+H]^+$; HRMS calcd. For $C_{26}H_{20}O_4N_2$: 423.5110, found: 423. 5143.

8-imino-4-oxo-2-phenyl-N-(1-phenylethyl)-4H,8H-pyrano[2,3-f]chromene-9-carboxamide (7j)

Off white solid; yield 71%; mp: 210–212°C; IR (KBr) ν_{max}: 3447, 3329, 3250, 3061, 2964, 2926, 1728, 1681, 1653, 1622, 1586, 1543, 1436, 1382, 1193, 1060, 836, 774, 686 cm^{-1}; ^1H NMR (400 MHz, $CDCl_3$) δ: 10.65 (d, 1H, *J* = 7.2 Hz, 12-NH), 9.04 (s, 1H, 10-H), 8.28 (d, 1H, *J* = 8.8 Hz, 5-H), 7.92 (d, *J* = 6.8 Hz, 2H, 2'-H and 6'-H), 7.86 (s, 1H, 8-NH), 7.55 (m, 3H, 3'-H, 4-H' and 5'-H), 7.36 (m, 5H, 2''-H, 3''-H, 4''-H, 5''-H and 6''-H), 7.16 (d, 1H, *J* = 8.8 Hz, 6-H), 6.84 (s, 1H, 3-H), 5.26 (q, *J* = 7.0 Hz 1H, 13-H), 1.60 (d, 3H, *J* = 6.8 Hz, 14-CH_3); ^{13}C NMR (100 MHz, $CDCl_3$) δ: 176.8 (C-4), 163.5 (C-2), 160.8 (C-6a), 157.1 (C-8), 156.4 (C-11), 153.2 (C-1a), 143.7 (C- 1''), 134.5 (C-1'), 132.2 (C-10), 130.9 (C-4'), 129.9 (C-5), 129.4 (C-3', 5'), 128.8 (C- 4''), 127.3 (C-2'', 6''), 126.3 (C-2', 6'), 126.1 (C-3'', 5''), 120.9 (C-4a), 120.0 (C-9), 113.4 (C-10a),

109.2 (C-6), 108.1 (C-3), 50.0 (C-13), 22.8 (C-14); ESI-MS *m/z*: 437.3 $[M+H]^+$; HRMS calcd. For $C_{27}H_{21}O_4N_2$: 437.5010, found: 437. 5021.

N-benzhydryl-8-imino-4-oxo-2-phenyl-4H,8H-pyrano[2,3-f]chromene-9-carboxamide (7k)

Off white solid; yield 63%; mp: 230–232°C; IR (KBr) ν_{max}: 3447, 3309, 2924, 2824, 1728, 1683, 1641, 1624, 1541, 1437, 1384, 1352, 1206, 1183, 1130, 1068, 829, 774, 702 cm^{-1}; ^1H NMR (400 MHz, $CDCl_3$) δ: 11.20 (br s, 1H, 12-NH), 9.11 (s, 1H, 10-H), 8.31 (d, 1H, *J* = 8.8 Hz, 5-H), 7.94 (d, *J* = 6.0 Hz, 2H, 2'-H and 6'-H), 7.88 (s, 1H, 8-NH), 7.56 (m, 3H, 3'-H, 4-H' and 5'-H), 7.36 (br s, 10H, 2"-H, 3"-H, 4"-H, 5"-H, 6"-H and 2'"-H, 3'"-H, 4'"-H, 5'"-H, 6'"-H), 7.19 (d, 1H, *J* = 8.8 Hz, 6-H), 6.86 (s, 1H, 3-H), 6.41 (d, *J* = 7.2 Hz,13-H); ^{13}C NMR (100 MHz, $CDCl_3$) δ: 176.8 (C-4), 163.5 (C-2), 160.8 (C-6a), 157.1 (C-8), 156.4 (C-11), 153.2 (C-1a), 143.7 (C- 1",1'"), 134.5 (C-1'), 132.2 (C-10), 130.9 (C-4'), 129.9 (C-5), 129.4 (C-3', 5'), 128.8 (C- 4", 4'"), 127.3 (C-2", 6" and C-2'", 6'"), 126.3 (C-2', 6'), 126.1 (C-3", 5" and C-3", 5'"), 120.9 (C-4a), 120.0 (C-9), 113.4 (C-10a), 109.2 (C-6), 108.1 (C-3), 52.0 (C-13); ESI-MS *m/z*: 499.7 $[M+H]^+$; HRMS calcd. For $C_{32}H_{23}O_4N_2$: 499.9110, found: 499.9081.

8-imino-N-(1-(4-methoxyphenyl)ethyl)-4-oxo-2phenyl-4H,8H-pyrano[2,3-f]chromene-9-carboxamide (7l)

Off white solid; yield 74%; mp: 218–220°C; IR (KBr) ν_{max}: 3445, 3309, 2924, 2823, 1730, 1683, 1641, 1624, 1541, 1437, 1384, 1352, 1206, 1183, 1130, 1068, 829, 774, 687 cm^{-1}; ^1H NMR (400 MHz, $CDCl_3$) δ: 10.57 (d, *J* = 5.6 Hz, 1H, 12-NH), 9.02 (s, 1H, 10-H), 8.25 (d, 1H, *J* = 8.4 Hz, 5-H), 7.91 (d, *J* = 6.0 Hz, 2H, 2'-H and 6'-H), 7.85 (s, 1H, 8-NH), 7.53 (br s, 3H, 3'-H, 4-H' and 5'-H), 7.32 (m, 2H, 2"-H and 6"-H), 7.14 (d, 1H, *J* = 8.4 Hz, 6-H), 6.88 (m, 2H, 3"-H and 5"-H),

6.82 (s, 1H, 3-H), 5.20 (m, 1H, 13-H), 3.78 (s, 3H, 4"-OCH_3), 1.57 (d, 3H, J = 6 Hz, 14-CH_3); ^{13}C NMR (100 MHz, $CDCl_3$) δ: 176.8 (C-4), 163.5 (C-2), 160.6 (C-6a), 158.7 (C- 4"), 157.1(C-8), 156.3 (C-11), 153.1 (C-1a), 135.8 (C- 1"), 134.3 (C-1'), 132.2 (C-10), 130.9 (C-4'), 129.8 (C-5), 129.4 (C-3', 5'), 127.3 (C-2", 6"), 126.3 (C-2', 6'), 120.9 (C-4a), 120.0 (C-9), 114.1 (C-3", 5"), 113.3 (C-10a), 109.1 (C-6), 108.1 (C-3), 55.3 (4"-O<u>C</u>H_3), 49.4 (C-13), 22.7 (C-14); ESI-MS *m/z*: 465.1 $[M-H]^+$; HRMS calcd. For $C_{28}H_{23}O_4N_2$: 465.0180, found: 465.0186.

N-(2,4-dimethoxybenzyl)-8-imino-4-oxo-2-phenyl-4H,8H-pyrano[2,3-f]chromene-9-carboxamide (7m)

Off white solid; yield 69%; mp: 213–215°C; IR (KBr) ν_{max}: 3449, 3309, 3066, 2926, 1728, 1683, 1649, 1624, 1508, 1438, 1385, 1353, 1206, 1154, 1130, 1071, 1036, 825, 774, 687 cm^{-1}; ^{1}H NMR (400 MHz, $CDCl_3$) δ: 10.47 (br s, 1H, 12-NH), 9.07 (s, 1H, 10-H), 8.28 (d, 1H, J = 8.8 Hz, 5-H), 7.95 (d, 2H, J = 6.4 Hz, 2'-H and 6'-H), 7.81 (s, 1H, 8-NH), 7.56 (m, 4H, 3'-H, 4-H', 5'-H and 6"-H), 7.15 (d, 1H, J = 8.8 Hz, 6-H), 6.85 (s, 1H, 3-H), 6.45 (m, 2H, 3"-H and 5"-H), 4.58 (d, 2H, J = 5.2 Hz, 13-CH_2), 3.86 (s, 3H, 2"-OCH_3), 3.79 (s, 3H, 4"-OCH_3); ^{13}C NMR (100 MHz, $CDCl_3$) δ: 177.0 (C-4), 163.6 (C-2), 161.4 (C-6a), 160.5 (C-4"), 158.7 (C-2"), 157.2 (C-8), 156.2 (C-11), 153.2 (C-1a), 134.2 (C-1'), 132.2 (C-10), 131.0 (C-4'), 130.1 (C-6"), 129.7 (C-5), 129.4 (C-3', 5'), 126.4 (C-2', 6'), 121.3 (C-4a), 120.0 (C-9), 118.9 (C-1"), 113.4 (C-10a), 109.2 (C-6), 108.2 (C-3), 103.9 (C-3"), 98.7 (C-6"), 55.5 (2", 4"-OCH_3), 39.3 (C-13) ; ESI-MS *m/z*: 483.7 $[M+H]^+$; HRMS calcd. For $C_{28}H_{23}O_6N_2$: 484.0040, found: 484.0051.

N-(2-bromobenzyl)-8-imino-4-oxo-2-phenyl-4H,8H-pyrano[2,3-f]chromene-9-carboxamide (7n)

Off white solid; yield 75%; mp: 211–213°C; IR (KBr) ν_{max}: 3436, 3328, 3058, 2925, 2854, 1729, 1680, 1651, 1622, 1436, 1385, 1350, 1353, 1195, 1069, 1028, 822, 774, 683 cm^{-1}; ^1H NMR (400 MHz, $CDCl_3$) δ: 10.70 (br s, 1H, 12-NH), 9.05 (s, 1H, 10-H), 8.27 (d, 1H, *J* = 8.8 Hz, 5-H), 7.93 (d, 2H, *J* = 6.4 Hz, 2'-H and 6'-H), 7.81 (s, 1H, 8-NH), 7.55 (m, 4H, 3'-H, 4-H' 5'-H and 3''-H), 7.45 (d, 1H, *J* = 7.6 Hz, 4''-H), 7.29 (m, 1H, 5''-H), 7.14 (m, 2H, 6-H and 6''-H), 6.84 (s, 1H, 3-H), 4.71 (d, 2H, *J* = 5.6 Hz, 13-H); ^{13}C NMR (100 MHz, $CDCl_3$) δ: 176.8 (C-4), 163.6 (C-2), 161.8 (C-6a), 157.2 (C-8), 156.2 (C-11), 153.2 (C-1a), 137.2 (C- 1''), 134.6 (C-1'), 132.9 (C-10), 132.2 (C-3''), 130.9 (C-4'), 130.0 (C-6''), 129.9 (C-5), 129.4 (C-3', 5'), 129.1 (C- 4''), 127.7 (C-5''), 126.4 (C-2', 6'), 123.8 (C-2''), 120.8 (C-4a), 120.0 (C-9), 113.4 (C-10a), 109.1 (C-6), 108.2 (C-3), 44.4 (C-13); ESI-MS *m/z*: 499.3 $[M+H]^+$; HRMS calcd. For $C_{26}H_{18}BrO_4N_2$: 499.0140, found: 499.0151.

N-(3-bromobenzyl)-8-imino-4-oxo-2-phenyl-4H,8H-pyrano[2,3-f]chromene-9-carboxamide (7o)

Off white solid; yield 78%; mp: 192–194°C; IR (KBr) ν_{max}: 3437, 3319, 3061, 2926, 2854, 1726, 1687, 1643, 1625, 1580, 1549, 1437, 1389, 1350, 1354, 1215, 1195, 1072, 824, 773, 686 cm^{-1}; ^1H NMR (400 MHz, $CDCl_3$) δ: 10.63 (br s, 1H, 12-NH), 9.05 (s, 1H, 10-H), 8.28 (d, 1H, *J* = 8.8 Hz, 5-H), 7.93 (m, 2H, 2'-H and 6'-H), 7.84 (s, 1H, 8-NH), 7.53 (m, 3H, 3'-H, 4-H' and 5'-H), 7.50 (br s, 1H, 2''-H), 7.39 (d, 1H, *J* = 7.6 Hz, 6''-H), 7.29 (d, 1H, *J* = 7.6 Hz, 4''-H), 7.20 (t, 1H, *J* = 8.0 Hz, 5''-H), 7.15 (d, 1H, *J* = 8.8 Hz, 6-H), 6.83 (s, 1H, 3-H), 4.62 (d, 2H, *J* = 6 Hz, 13-H); ^{13}C NMR (100 MHz, $CDCl_3$) δ: 176.8 (C-4), 163.6 (C-2), 161.9 (C-6a), 157.2 (C-8), 156.2 (C-11), 153.2 (C-1a), 140.6 (C- 1''), 134.7 (C-1'), 132.9 (C-10), 132.2 (C-2''), 130.9 (C-4'), 130.5 (C-5''), 130.3 (C-4''), 130.0 (C-5), 129.4 (C-3', 5'), 126.4 (C-2', 6'), 126.2 (C-6''), 122.8 (C-3''), 120.7

(C-4a), 120.0 (C-9), 113.4 (C-10a), 109.1 (C-6), 108.2 (C-3), 43.4 (C-13); ESI-MS *m/z*: 499.3 $[M+H]^+$; HRMS calcd. For $C_{26}H_{18}BrO_4N_2$: 499.0171, found: 499.0176.

N-(2-chlorobenzyl)-8-imino-4-oxo-2-phenyl-4H,8H-pyrano[2,3-f]chromene-9-carboxamide (7p)

Off white solid; yield 80%; mp: 211–213°C; IR (KBr) ν_{max}: 3438, 3303, 3292, 3058, 2924, 2853, 1728, 1677, 1648, 1621, 1585, 1539, 1437, 1386, 1353, 1194, 1071, 1053, 830, 774, 686 cm^{-1}; ^1H NMR (400 MHz, $CDCl_3$) δ: 10.68 (t, 1H, 12-NH), 9.04 (s, 1H, 10-H), 8.27 (d, 1H, *J* = 8.8 Hz, 5-H), 7.92 (dd, 2H, *J* = 6.0, 1.6 Hz, 2'-H and 6'-H), 7.88 (br s, 1H, 8-NH), 7.54 (m, 3H, 3'-H, 4-H' and 5'-H), 7.45 (dd, 1H, *J* = 6.8, 1.6 Hz, 3''-H), 7.38 (dd, 1H, *J* = 6.8, 1.6 Hz, 6''-H), 7.23 (m, 2H, 4''-H, 5''-H), 7.14 (d, 1H, *J* = 8.8 Hz, 6-H), 6.83 (s, 1H, 3-H), 4.73 (d, 2H, *J* =5.6 Hz, 13-H); ^{13}C NMR (100 MHz, $CDCl_3$) δ: 176.8 (C-4), 163.6 (C-2), 161.8 (C-6a), 157.2 (C-8), 156.2 (C-11), 153.2 (C-1a), 135.6 (C- 1''), 134.6 (C-1'), 133.7 (C-2''), 132.2 (C-10), 130.9 (C-4'), 130.0 (C-6''), 129.7 (C-5), 129.6 (C-3''), 129.4 (C-3', 5'), 128.9 (C- 4''), 127.1 (C-5''), 126.3 (C-2', 6'), 120.8 (C-4a), 120.0 (C-9), 113.4 (C-10a), 109.1 (C-6), 108.2 (C-3), 42.0 (C-13); ESI-MS *m/z*: 457.5 $[M+H]^+$; HRMS calcd. For $C_{26}H_{18}ClO_4N_2$: 458.0141, found: 458.0146.

N-(3-chlorobenzyl)-8-imino-4-oxo-2-phenyl-4H,8H-pyrano[2,3-f]chromene-9-carboxamide (7q)

Off white solid; yield 75%; mp: 184–186°C; IR (KBr) ν_{max}: 3436, 3301, 3304, 2924, 2854, 1727, 1686, 1658, 1626, 1553, 1449, 1437, 1385, 1348, 1196, 1069, 827, 772, 683 cm^{-1}; ^1H NMR (400 MHz, $CDCl_3$) δ: 10.54 (br s, 1H, 12-NH), 8.97 (s, 1H, 10-H), 8.19 (d, 1H, *J* = 8.4 Hz, 5-H), 7.84 (d, 2H, *J* = 6.0 Hz, 2'-H and 6'-H), 7.76 (s, 1H, 8-NH), 7.41 (m, 3H, 3'-H, 4'-H and 5'-H), 7.17

(m, 4H, 2''-H, 4''-H, 5''-H and 6''-H), 7.09 (d, 1H, *J* = 8.8 Hz, 6-H), 6.75 (s, 1H, 3-H), 4.54 (d, 2H, *J* =5.2 Hz, 13-H); ^{13}C NMR (100 MHz, $CDCl_3$) δ: 176.8 (C-4), 163.6 (C-2), 161.9 (C-6a), 157.2 (C-8), 156.3 (C-11), 153.2 (C-1a), 140.3 (C- 1''), 134.8 (C-1'), 134.6 (C-10), 132.2 (C-3''), 130.9 (C-4'), 130.1 (C-5''), 130.0 (C-5), 129.4 (C-3', 5'), 127.6 (C-4''), 127.6 (C-2''), 126.4 (C-2', 6'), 125.7 (C-6''), 120.6 (C-4a), 120.0 (C-9), 113.4 (C-10a), 109.1 (C-6), 108.2 (C-3), 43.4 (C-13); ESI-MS *m/z*: 457.5 $[M+H]^+$; HRMS calcd. For $C_{26}H_{18}ClO_4N_2$: 458.0243, found: 458.0247.

N-(4-(tert-butyl)benzyl)-8-imino-4-oxo-2-phenyl-4H,8H-pyrano[2,3-f]chromene-9-carboxamide (7r)

Off white solid; yield 61%; mp: 210–212°C; IR (KBr) ν_{max}: 3439, 3363, 2958, 2925, 2855, 1729, 1681, 1644, 1548, 1436, 1384, 1352, 1195, 1073, 828, 774, 685 cm^{-1}; ^{1}H NMR (400 MHz, $CDCl_3$) δ: 10.41 (t, 1H, 12-NH), 8.95 (s, 1H, 10-H), 8.15 (d, 1H, *J* = 8.8 Hz, 5-H), 7.81 (d, 2H, *J* = 5.6 Hz, 2'-H and 6'-H), 7.70 (s, 1H,8-NH), 7.42 (m, 3H, 3'-H, 4-H' and 5'-H), 7.25 (d, 2H, *J* = 8.0 Hz, 2''-H, 6''-H), 7.17 (d, 2H, *J* = 8.0 Hz, 3''-H, 5''-H), 7.02 (d, 1H, *J* = 8.8 Hz, 6-H), 6.72 (s, 1H, 3-H), 4.51 (d, 2H, *J* = 5.6 Hz, 13-H), 1.17 (s, 9H, 4''-$C(CH_3)_3$); ^{13}C NMR (100 MHz, $CDCl_3$) δ: 176.9 (C-4), 163.6 (C-2), 161.7 (C-6a), 157.2 (C-8), 156.2 (C-11), 153.2 (C-1a), 150.4 (C- 4''), 135.1 (C- 1''), 134.5 (C-1'), 132.2 (C-10), 131.0 (C-4'), 129.9 (C-5), 129.4 (C-3', 5'), 127.4 (C-2'', 6''), 126.4 (C-2', 6'), 125.7 (C-3'', 5''), 120.9 (C-4a), 120.0 (C-9), 113.4 (C-10a), 109.2 (C-6), 108.2 (C-3), 43.70 (C-13), 34.6 (3'-$\underline{C}(CH_3)_3$), 31.4 (3'-$C(\underline{C}H_3)_3$); ESI-MS *m/z*: 480.4 $[M+H]^+$; HRMS calcd. For $C_{30}H_{27}O_4N_2$: 480.3840, found: 480. 3843.

8-imino-N-(2-(2-methoxyphenoxy)ethyl)-4-oxo-2-phenyl-4H,8H-pyrano[2,3-f]chromene-9-carboxamide (7s)

Off white solid; yield 71%; mp: 178–180°C; IR (KBr) ν_{max}: 3446, 3310, 3066, 2926, 1730, 1685, 1649, 1624, 1580, 1438, 1384, 1352, 1255, 1221, 1195, 1124, 830, 774, 687 cm^{-1}; ^1H NMR (400 MHz, $CDCl_3$) δ: 10.53 (br s, 1H, 12-NH), 9.05 (s, 1H, 10-H), 8.28 (d, 1H, *J* = 8.4 Hz, 5-H), 7.95 (d, 2H, *J* = 6.0 Hz, 2'-H and 6'-H), 7.85 (s, 1H, 8-NH), 7.56 (br s, 3H, 3'-H, 4'-H and 5'-H), 7.16 (d, 1H, *J* = 8.4 Hz, 6-H), 6.91 (m, 5H, 3-H, 3"-H, 4"-H, 5"-H, 6"-H), 4.23 (br s, 2H, 13-CH_2), 3.87 (br s, 5H, 14-CH_2, 2"-OCH_3); ^{13}C NMR (100 MHz, $CDCl_3$) δ: 176.8 (C-4), 163.6 (C-2), 162.0 (C-6a), 157.2 (C-8), 156.3 (C-11), 153.2 (C-1a), 150.0 (C-1"), 148.1 (C-2"), 134.4 (C-1'), 132.2 (C-10), 131.0 (C-4'), 130.0 (C-5), 129.4 (C-3', 5'), 126.4 (C-2', 6'), 122.0 (C-5"), 121.1 (C-4a), 120.0 (C-9), 114.9 (C-4"), 113.4 (C-10a), 112.4 (C-6"), 110.4 (C-3"), 109.1(C-6), 108.2 (C-3), 68.1(C-14), 56.1(2"-OCH_3), 39.6 (C-13); ESI-MS *m/z*: 483.7 $[M+H]^+$; HRMS calcd. For $C_{28}H_{23}O_6N_2$: 484.0120, found: 484. 0123.

BIOLOGICAL EVALUATION

Inhibition assays of AChE and BuChE

To assess the inhibition potency of compounds against cholinesterases (ChE), all target compounds were subjected to spectrophotometric method of Ellman et al.[34, 35] The assay for inhibition of AChE and BuChE was performed as described in the following procedure; in 96-well plate, 10 µL of test sample , 145 µL phosphate buffer 200 mM (pH 7.7), 80 µL of DTNB (18.5 mg of DTNB dissolved in 10 mL phosphate buffer pH 7.7), and 10 µL of enzyme (0.4 U/mL) was pre incubated for 5 minutes at 37 °C before adding substrate. Subsequently, by addition of 15 µL of 1 mM of ATCh or BTCh (according to the respective enzyme) the enzymatic reaction was developed for 5 min at 37 °C. In order to obtain inhibition curve, at least five different concentrations of the test compounds were assayed at 412 nm, each concentration

in triplicate. Serving as a blank, an identical reaction solution without the inhibitor was processed using the same protocol to yield 100% of AChE or BChE activities. IC_{50} values were determined graphically by plotting the percentage enzyme activity (100% for the reference) versus logarithm of test compound concentration.

Kinetic characterization of AChE inhibition

For the determination of inhibition model and inhibition constant Ki, for compound **7s,** kinetic characterization of AChE inhibition was performed based on a reported method.[36] The LineweavereBurk plots were generated by using Graph pad prism version 5 at fixed amount of AChE and varying amounts of the substrate ATCh (0.1-0.5 mM) and in the absence or presence of different inhibitor concentrations of **7s (**0.1, 0.4 and 1 μM). The kinetic experiments were performed similar to enzyme inhibition assay. The assay solution consists of 145 μL of 200 mM phosphate buffer (pH 7.7), 80 μL of DTNB (18.5 mg of DTNB dissolved in 10 mL phosphate buffer pH 7.7) and 10 μL of 0.4 units/mL AChE. Three different concentrations of inhibitor **7s** was added to the assay solution and pre-incubated for 5 min at 25 ^{0}C. The enzymatic reaction was initiated by the addition of ATCh (15 μL) in different concentrations and the mixture was again incubated for 5 min. Kinetic characterization of hydrolysis was monitored at 412 nm over 6 min. The parallel control experiments were carried out without inhibitor. The re-plots of the slopes and intercepts of the double reciprocal plots against inhibitor concentrations gave the inhibitor constants (Ki1 and Ki2, for the binding to free enzyme and enzyme substrate complex) as the intercepts on the negative x-axis. Data analysis was performed using Microsoft Excel.

Antioxidant Activity Assay

The ABTS scavenging activity assay was performed to assess the compounds for their antioxidant activity.[37] ABTS stock solution (8mM) was prepared by dissolving 44mg ABTS in 10mL Millipore water. ABTS radical cation ($ABTS^{\bullet+}$) was generated by adding 3mM potassium persulfate to the ABTS stock solution in equal volumes and keeping it in the dark at room temperature for 12-18 h. $ABTS^{\bullet+}$ work solution was prepared freshly before the experiment in 1:29 ratio with methanol. The 10 μL of the test compounds were allowed to react with 290 μL of $ABTS^{\bullet+}$ solution. The plate was placed in the wells of a 96 well plate microplate reader and the absorbance was recorded 30 min after initial mixing at 734 nm. The plate was automatically shaken prior to each reading. Trolox was used as a standard. A blank using phosphate buffer instead of antioxidant and trolox was carried out in each assay. To obtain IC_{50} data each experiment was performed in thrice, averaged and reported in the form of mean ± S.E.M.

ThT fluorescence assay

Thioflavin T-based flurometric assay (ThT) was performed to identify Aβ aggregates with high sensitivity.[22, 38] The β-Amyloid$_{1–42}$ ($A\beta_{1–42}$) and Thioflavin T were purchased from sigma USA. Then the $A\beta_{1–42}$ was solubilized in dry DMSO to a final stock concentration of 200 μM. The stock solution was centrifuged at the speed of 12,000 rpm for 10 min and supernatant that obtained was kept frozen at -80 °C until use for experiments. The solutions of 2.0 mM target flavone analogs were prepared in DMSO for storage and diluted at in phosphate-buffered saline (PBS at pH 7.4) before use. The reaction mixture was prepared at fixed concentration of 2 μL of 200 mM $A\beta_{1–42}$ and 2 μL of target flavone analogs at different concentrations (0.02 - 0.1mM) in 76 μL of phosphate-buffered saline (PBS at pH 7.4). After the incubation for 24 h at room temperature, 80 μL of 5 μM ThT solution (in 50 mM glycine-NaOH at pH 8.5) was added to the

reaction solution. The potential interaction between target flavone analogs with $A\beta_{1-42}$ was performed by LS-55 spectrofluorimeter (PerkinElmer, USA), with 1.0 cm quartz cells. Fluorescence emission spectra were recorded at 25 ^{o}C with a wavelength range of 410–600 nm and excited at 390nm. The bandwidth was fixed to 5.0 nm for both excitation and emission. The independent experiments were performed thrice and each time identical spectra were obtained.

Cell Viability Assay

Human neuroblastoma (*SK-N-SH*) cells were obtained from National Centre for Cell Sciences (NCCS), Pune, India. The SK-N-SH cells were cultured in minimal essential medium (MEM) containing 0.5 mM L-glutamine, 0.1 mM sodium pyruvate and 1 mM non-essential amino acids and 10% Fetal bovine serum (FBS) and maintained at 37 ^{0}C in humidified incubator under 5% CO_2 / 95% air. When SK-N-SH cells' reached 80% confluence, and then were used in the following *in vitro* experiments. SK-N-SH cells' were seeded in 96-well plates at the quantity of 0.2×10^6 cells per well. The cells were treated with test compounds or galantamine in increasing concentrations of 40, 80 and 120 μM for 24 h in humidified CO_2 incubator with 5% CO_2 at 37 °C for 24 h. At the end, 20 μL of MTT at a final concentration of 5 mg/mL was supplemented and incubated for an additional 4 h in humidified atmosphere followed by the addition of 200 μL of DMSO to the wells to dissolve the MTT formazan crystals. In a control experiment, cells were grown in a same media without test compounds. Absorbance was recorded at 570 nm immediately after the development of purple colour. The formazan generated in the control cells was considered to represent 100% viability. Relative cell viability was evaluated according to the quantity of MTT converted into insoluble formazan salt.[39] Three self-determining experiments

were carried out and mean ± S.E.M was calculated and reported as (%) of cell viability vs concentration (μM).

Protection against H_2O_2 induced cell death in SK-N-SH **cells**

To measure neuroprotective effect of selected test compounds against H_2O_2 induced oxidative injury in SK-N-SH cells,

MTT assay was performed as described earlier.[39] Thus, SK-N-SH cells were pre-treated with different concentrations of test compounds 40, 80 and 120 μM and galantamine for 3 h before treatment with H_2O_2 in a humidified CO_2 incubator with 5% CO_2. To induce oxidative stress, 1.0 mM H_2O_2 was added to the medium and incubated for 24 h in humidified atmosphere. Further the cell viability was measured by MTT colorimetry as described above.

Fluorescence spectroscopy

All fluorescence measurements[40] were carried out with Perkin Elmer LS55 fluorescence spectrometer using 1.0 cm quartz cell to determine quantitatively potential interactions between flavones analog and AChE. The fluorescence emission spectra were recorded at 25 ^{o}C, in the wavelength range from 300 to 500 nm, with an excitation wavelength of 285 nm. The slit width of 5.0 nm is set for both excitation and emission. The scan speed was adjusted to100 nm/min. The experiments were carried at the fixed AChE concentration (0.001 mM) and different concentrations of flavone derivatives from 0.001 to 0.009 mM in 0.1M phosphate buffer solution at the physiological pH of 7.4. The samples were allowed to equilibrate for 5 min after each

addition. The binding constant were calculated using the maximum fluorescence value at 350 nm for AChE. Three independent experiments were performed at each time and identical spectra were recorded.

Circular dichroism (CD)

Determination of conformational changes of AChE with different concentrations of flavone derivatives was carried out on JASCO J-1500 CD spectrometer using a quartz cell with a path length of 0.1 cm cell in a nitrogen atmosphere. Three scans were accumulated at a scan speed of 100 nm min^{-1}, with data being collected at room temperature for every 0.5 nm in the range of 190 to 260 nm. All the parameters were followed according to our previous procedures.[41] For CD studies, the final concentration of 0.001 mM AChE and 1μL of test compounds with varied concentrations (0.001, 0.005 and 0.009 mM) were used. After 5 min incubation, spectra was recorded. Each experiment is repeated thrice and the result was averaged. The percentage of relative contents of secondary structure; α- helix, β-sheets and random coils were calculated using CDNN 2.1, a web based software.

Autodock analysis

Since the experimental evidence showed flavone derivatives binding to AChE and also superior at inhibiting the AChE, we were fascinated in exploratory the probable binding mechanism and important interactions in atomic details in the binding site via molecular docking. The Autodock program (version 4.2.3) was used to perform the molecular docking of flavone derivatives binding to AChE according to earlier studies. [42, 43] To obtain the binding site and type of interactions involved in the formation of Ligand-protein complexes; in the present study,

Lamarckian genetic algorithm (LGA) was implemented to calculate the possible conformation of the drug that binds to the proteins.[44] Many reports discussed that, LGA is to be the best performing method of docking in terms of its ability in finding the least energy and also showed the accuracy in the structure prediction; it also includes the ligand flexibility.[42] The known crystal structure of electric eel acetylcholinesterase (EeAChE, PDB Id: 1C2O) was retrieved from the Brookhaven Protein Data Bank. The three-dimensional structure (3D) of flavones derivatives were built from its two-dimensional structure (2D), and its geometry was optimized using Discovery studio 3.5 software in the Insight-II/Builder program. In Auto Dock (4.2.3) program water molecules and ions were removed (including ordered water molecules) and hydrogen atoms were added to functional groups with the appropriate geometry within the protein, in order to get proper protonation state of active site of the protein which was ionized as required at physiological pH. To describe all binding sites and to have structural efforts, blind docking was carried out using a grid based procedure. Now the output was saved as a PDBQT. Grid box is set and output is saved as a .gpf file. The docking area was defined by a grid spacing of 1.00 Å and dimensions of (126 X 126 X 126) with points along the x, y and z axes. The docking parameters used were; number of genetic algorithm (GA) runs: 30, individual population size: 150, maximum number of energy evaluations: 2500000, maximum number of generations: 27000, maximum number of top individuals that automatically survive: 1, rate of genetic mutation: 0.02, rate of crossover: 0.8, GA crossover mode: two points, output is selected as Lamarckian GA (4.2) and file is saved as .dpf. Among 30 conformations the conformer with the least free energy which is close to the experimental free energy was considered for the analysis of binding site and binding mode. [45]

RESULTS AND DISCUSSION

Chemistry

The synthetic route to target flavone derivatives (**7a**–**s**) starting from commercially available resorcinol is shown in Scheme 1. Resacetophenone (**1**) was easily achieved by acetylation of readily available precursors, such as resorcinol, $ZnCl_2$ and acetic acid,[27, 28] which was on reaction with benzoyl chloride afforded 1-(4-benzoyloxy-2-hydroxyphenyl)-3-phenyl-1,3-propanedione (**2**).[29, 30] Subsequently, treatment of **2** with Conc. H_2SO_4 followed by 5% K_2CO_3 gave the desired 7-hydroxyflavone backbone (**3**) at a yield of 67%.[31] Next, 8-formyl-7-hydroxyflavone (**4**) was accomplished by Duff formylation in an acidic medium between 7-hydroxyflavone (**3**) and hexamethylenetetramine (HMTA) under microwave irradiation at 300 W for 7 min.[32] A series of N-substituted cyanoacetamide derivatives (**6a**–**s**) were readily prepared by treating different amines with equivalent amount of ethylcyanoacetate (**5**) as described in our recent publication.[21, 22] Finally, the key intermediate 8-formyl-7-hydroxyflavone (**4**) was reacted with the corresponding N-substituted cyanoacetamides (**6a**–**s**) in the presence of Et_3N to provide the target products (**7a**–**s**).[33] All new compounds showed analytical and spectroscopic data (IR, ^1H NMR, ^{13}C NMR and Mass) in good agreement with their structures, as detailed in the experimental section and then submitted to biological evaluation.

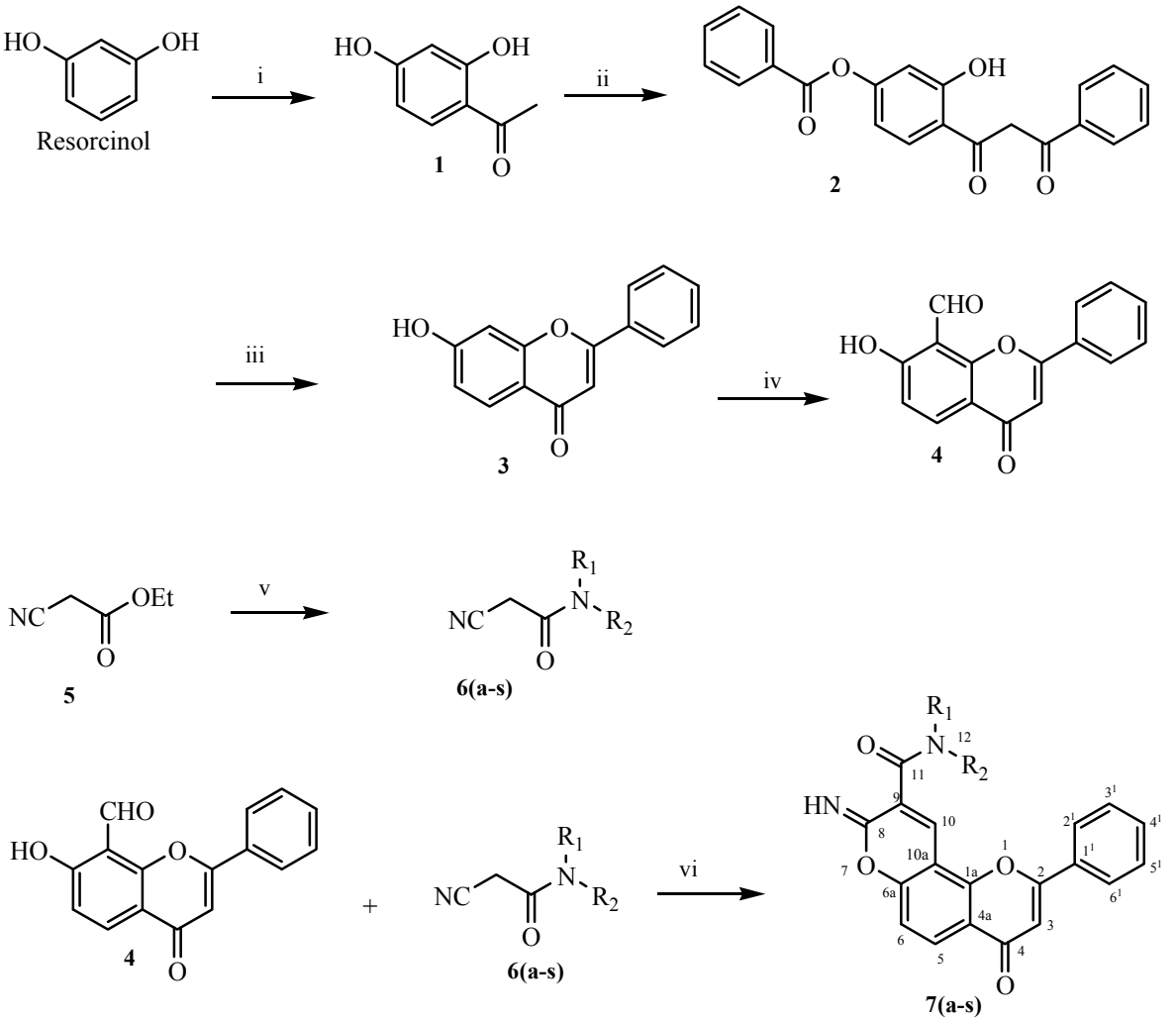

Scheme 1. Reagents and conditions: (i) $ZnCl_2$, GAA, 140-150^{0}C; (ii) K_2CO_3, dry acetone, benzoyl chloride, 20h, reflux (iii) a. H_2SO_4, 4h, 5^{0}C; b. 5% K_2CO_3, con HCl (iv) HMTA, GAA; MW, 300W, for 7min, 20% HCl, 200W for 4min; (v) corresponding amine, EtOH (vi) Et_3N, EtOH.

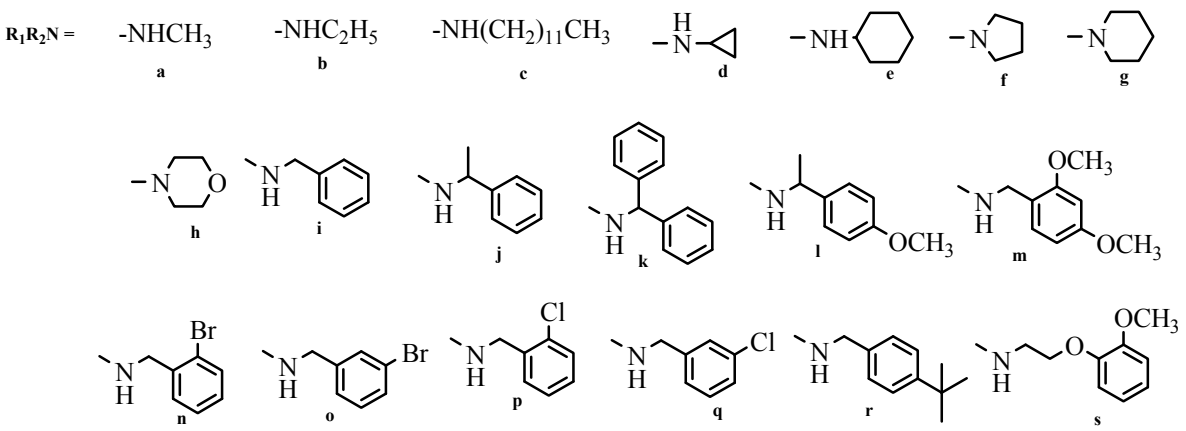

BIOLOGY

In vitro cholinesterase inhibition activity

To evaluate the potential of the target flavone derivatives **7a**–**s** for the management of AD, their cholinesterase inhibitory activities were evaluated by following method of Ellman et al with minor changes using AChE from *Electrophorus electricus* (*E*AChE) ans BuChE from Equine serum (BuChE),[34, 35] with commercially available Galantamine, Tacrine, Donepezil and Rivastigmine as reference standards. Table 1 illustrates the anticholinesterase potency of compounds as expressed in IC_{50} values and selectivity index.

Table 1. An *in vitro* AChE and BuChE inhibitory activities and ABTS radical scavenging capacities by the test compounds, and their selectivity index.

	IC_{50} (μM) ± S.E.M.[a]			IC_{50} (μM) ± S.E.M.[c]
Compounds	AChE	BuChE	Selectivity for AChE[b]	ABTS radical scavenging activity
7a	0.418 ± 0.019	>100	–	>50
7b	0.338 ± 0.005	>100	–	>50
7c	0.344 ± 0.013	>100	–	>50

7d	0.337 ± 0.022	80.0 ± 5.78	237.38	>50
7e	0.438 ± 0.042	>100	–	29.34 ± 1.2
7f	0.305 ± 0.011	90.0 ± 9.89	295.08	>50
7g	0.375 ± 0.023	NA	–	>50
7h	0.469 ± 0.033	NA	–	>50
7i	0.581 ± 0.028	35.0 ± 2.45	60.24	16.24 ± 1.59
7j	0.273 ± 0.002	35.84 ± 3.46	131.28	26.40 ± 1.21
7k	1.006 ± 0.075	NA	–	44.81 ± 0.77
7l	0.694 ± 0.077	>100	–	>50
7m	0.811 ± 0.097	25.37 ± 3.46	31.28	>50
7n	0.286 ± 0.010	87.43 ± 9.81	305.69	28.35 ± 0.75
7o	0.280 ± 0.003	77.36 ± 6.65	276.28	38.46 ± 3.48
7p	0.406 ± 0.023	57.30 ± 4.21	141.13	31.80 ± 3.55
7q	0.547 ± 0.04	17.93 ± 1.29	32.77	42.34 ± 4.80
7r	0.291 ± 0.007	57.93 ± 1.81	221.95	49.84 ±5.2
7s	0.271 ± 0.012	>100	–	>50

Galantamine	0.670 ± 0.025	19.85 ± 0.92	29.62	–
Donepezil	0.036 ± 0.018	7.69 ± 0.45	213.61	–
Tacrine	0.385 ± 0.162	1.85 ± 0.2	4.80	–
Rivastigmine	3.45 ± 0.92	5.56 ± 1.5	1.61	–
Trolox	–	–	–	27.35 ± 1.34

[a] Inhibitor's concentration that inhibits 50% of enzyme activity (mean ± SD). [b]Selectivity ratio = (IC_{50} of BuChE)/(IC_{50} of AChE). [C]Data expressed as IC_{50}, the test compound's concentration that inhibits 50% of free radicals (mean ± SD).

All tested target compounds displayed good inhibitory activity against AChE with IC_{50} values in the sub micro molar range. Almost all the compounds exhibited moderate to weak activity against BuChE and showed higher selectivity for AChE over BuChE. It is evident from the IC_{50} values of compounds that most of the analogs with different amide moieties showed little fluctuation on the inhibitory activities of AChE.

From the data, it is notable that compounds **7j**, **7n**, **7o**, **7r** and **7s** showed most potent inhibition for AChE with IC_{50} values in 0.2 μM range much better than that of tacrine. Compounds **7b**, **7c**, **7d**, **7f** and **7g** have shown comparable potency to that of tacrine. Except **7k**, **7l** and **7m**, all the compounds exhibited 2.47 to 1.15 fold higher AChE inhibitory activity than galantamine.

As far as BuChE concern, except **7q** with IC_{50} value 17.93 ± 1.29, all compounds displayed lesser potency than galantamine. Interestingly, most of the active analogs such as **7d, 7f**, **7j**, **7n**, **7o**, **7p** and **7r** showed good inhibition selectivity against AChE over BuChE than tacrine by 63.68 to 6.51 fold. The most active analogs **7j**, **7n**, **7o** and **7r** also displayed higher AChE

inhibition selectivity (131.28 to 305.69) than galantamine (29.62). This selectivity profile might be beneficial to diminish peripheral cholinergic side effects and provide lower toxicity. Because severe side effects of AChE inhibitors, such as tacrine, have been suggested to be attributed to their poor selectivity. On the other hand, compounds **7i**, **7m** and **7q** could be considered as dual inhibitors as they inhibited significantly the activity of both the enzymes. From these observations, compounds **7j**, **7n**, **7o**, **7r** and **7s** were selected for further studies.

Kinetic study of the AChE inhibition

For better characterizing AChE inhibitory properties of this family of compounds, a kinetic assessments were performed with the potent inhibitor **7s** using EeAChE. The results of this study was summarized in Figure 1a. The assessment was performed by means of steady-state inhibition (Lineweaver-Burk plots of initial velocity) of *Ee*AChE using acetylthiocholine iodide as substrate. Lineweaver-Burk plots displayed both increased slopes (decreased Vmax) and intercepts (higher Km) at increasing concentration of the inhibitor, which indicated a mixed-type inhibition.[36] The inhibitory constants (K_{i1} and K_{i2}) for the compound **7s** were calculated as 0.433 μM (binding to free enzyme) and 0.400 μM (binding to enzyme–substrate complex) using secondary plots (Figure 1b & 1c).

Figure 1 (here)

In vitro **antioxidant activity**

The antioxidant activities of all the new flavones derivatives were evaluated by using well established radical scavenging assay method using ABTS,[37] the vitamin E analog trolox was used as a reference. The antioxidant activity was expressed in IC_{50} values. As shown in Table 1, nine synthetic analogs were found to possess moderate to good ABTS radical scavenging

capacities ranging from 16.24 to 49.84 μM. Compounds **7i** and **7j** showed most potent ABTS radical scavenging activities with IC_{50} values of 16.24 and 26.40 μM, respectively which was higher than that of trolox (IC_{50} = 27.35 μM). On the other hand, **7e**, **7n** and **7p** exhibited comparable potency to that of trolox, however, compounds **7k**, **7o**, **7q** and **7r** had less radical scavenging capacity with that of trolox. Remaining ten compounds were disclosed poor antioxidant activities with IC_{50} values greater than 50 μM.

Effect on the Aβ aggregation

To investigate the effects of the flavones derivatives and galantamine on self-induced $A\beta_{1-42}$ aggregation, some compounds that showed good potency for AChE inhibition were selected and assessed via the thioflavin T fluorescence method.[38] In the assay, the fluorescence emission maximum for $A\beta_{1-42}$ was obtained at 450 nm. With the increasing concentrations of galantamine, the fluorescence maxima of $A\beta_{1-42}$ decreased gradually (Figure 2a), which reveals galantamine quenched the intrinsic fluorescence of $A\beta_{1-42}$. In contrast, after incubation of increasing concentrations of **7j**, **7n**, **7o**, **7r** and **7s** (0.02, 0.06, 0.1 mM) with a fixed concentration of $A\beta_{1-42}$, a gradual enhancement in the fluorescence intensity of ThT at 450 nm was occurred in dosage-dependent manner upon interaction (Figure 2b, 2c and 2d) (**7r** and **7s** were shown in Figure S1 in Supplementary Information). It has been reported that the hydrogen bonds are crucial for the co-assembly between ligand and $A\beta_{1-42}$ aggregates interactions.[46, 47] Thus, acceleration of the aggregation may be attributed to non covalent interactions between hydrophilic ends of **7j**, **7n**, **7o**, **7r** and **7s** and amide and carboxylic groups of Aβ peptide.[48] These interactions convert the Aβ monomers and oligomers into aggregates and alleviate the Aβ-induced toxicity, since

oligomers accounted to be more toxic forms to neurons in comparison with the fibril aggregates.[49] Hence, this $A\beta_{1-42}$ aggregation modulating ability of target compounds eventually benefit the treatment of AD.

Figure 2 (here)

Cell viability in SK-N-SH cells

To gain insight into the therapeutic potential of these derivatives, cell viability and neuroprotective capacity against oxidative stress were assayed using the human neuroblastoma cell line SK N SH.[39] Compounds **7j**, **7n**, **7o**, **7r** and **7s** with highest potency for AChE inhibition activity were selected as representative compounds. First, to examine the potential cytotoxic effect of **7j**, **7n**, **7o**, **7r**, **7s** at 40, 80 and 120 μM concentrations in comparison with galantamine, the calorimetric MTT assay was performed. Our results showed that all the tested compounds were nontoxic to SK-N-SH cells at lower (40 μM) concentrations (Figure 3). Interestingly, compound **7r** is nontoxic to SK-N-SH cells at all the concentrations, similar to galantamine. In addition, compounds **7j** and **7s** were nontoxic than reference galantamine at lower concentrations (40 & 80 μM), however, showed 70 % and 60 % cell viability, respectively at the high concentration (120 μM).

Figure 3 (here)

Neuroprotective effect against H_2O_2 induced cell death in SK-N-SH cells

Then compounds **7j**, **7n**, **7o**, **7r** and **7s** were tested for their capacity to protect human SK-N-SH neuroblastoma cells against oxidative stress-associated death induced by H_2O_2 using MTT assay [39] Galantamine and catechin were used as reference compounds. In this assay, treatment of cells with 1.0 mM H_2O_2 for 24 h reduced the cell viability to 40% as compared to the control. The gained data are shown in Figure 4. Pretreatment of SK-N-SH cells for 3 h with compounds

7j, **7n**, **7o**, **7r** and **7s** at different concentrations 40, 80 and 120 μM prior to the H_2O_2 insult significantly protected the neurons against H_2O_2-induced cell death. As can be seen in Figure 4, compounds **7j**, **7r** and **7s** exhibited neuroprotective effects at low concentrations (40 and 80 μM). Compounds **7n** and **7o** displayed lower protective capability than reference compounds. These observations further indicated that these new flavones derivatives act as potential oxidative suppressors.

Figure 4 (here)

Fluorescence Emission Data Analysis

Anti AD drugs are known to bind to AChE with high affinity, so it is necessary to understand the protein drug interactions, as flavone derivatives **7j**, **7n**, **7o**, **7r** and **7s** found to be potent AChE inhibitors. The Fluorescence emission spectroscopy is the appropriate research tool to understand protein drug interactions and also to quantify binding constants, free energies, number of binding sites and intermolecular distances.[50]

AChE showed a strong fluorescence emission maximum at 350 nm (λ_{ex} = 285 nm). The addition of target compounds to AChE resulted in change in fluorescence. Figure 5 (**7s** was shown in Figure S2 in Supplementary Information) showed the fluorescence emission spectra in the absence and presence of target compounds at various concentrations (0.001 to 0.009 mM) and unchanging concentration of AChE (0.001mM). Increasing the target compound concentrations resulted in a lowering of AChE fluorescence intensity with slight decrease in maximum emission. Previously it has been stated that the intrinsic fluorescence of AChE was mainly contributed by the tryptophan residue alone, since phenylalanine gives a very low quantum yield, and tyrosine fluorescence emission is almost totally quenched if it is ionized. Hence, the decrease in concentration-dependent quenching of intrinsic fluorescence of AChE suggested the formation

of complex between flavones derivatives and AChE which changed the microenvironment around the vicinity of tryptophan residue.[51] Moreover, an increasing concentration of target compounds with AChE, the increasing absorbance of excitation and or emission radiation causes inner filter effect that may develops the nonlinear relationship between the observed fluorescence intensity and the concentration of target compounds. This effect was corrected using the following equation.[50]

$$F_{cor} = F_{obs}10\ (A_{ex} + A_{em}) / 2$$

Here, F_{cor} is the corrected fluorescence intensity; A_{ex} and A_{em} are the absorbance of fluorescence excitation nm and emission wavelengths at 285 and 350 nm, respectively for AChE, F_{obs} is the observed fluorescence.

In a broad perspective, the mechanism of quenching is classified into dynamic and static quenching. The dynamic quenching is a result of collision encounters between the fluorophore and the quencher, whereas static quenching refers to complex formation between fluorophore and quencher. These quenching mechanisms are distinguished by temperature, viscosity and/or by fluorescence life time. In order to understand the fluorescence quenching mechanism (static or dynamic) in AChE-flavone derivative complexes, here we have plotted F0/F against Q.[52] The resulting plots are linear for AChE-flavone derivative complexes (see Figure S3 in the Supporting Information) recommending that the quenching is majorly static quenching via formation of flavone derivatives–AChE complexes.

In favor of static quenching, the binding constant (Ks) and the number of binding sites (n) can be developed from the following modified Stern-Volmer equation.[53, 54]

$$\text{Log}\ [(F0\text{-}F/F)] = \log K_S + n \log [Q]$$

Where Q is quencher concentration, n is the slope and corresponds to number of binding sites and Ks is the binding constant. From the above equation, the n values were calculated to be 0.80, 0.76, 0.85, 0.99 and 0.80 for **7j**, **7n**, **7o**, **7r** and **7s**, respectively suggesting that AChE interacts with different flavone derivatives in a one-to-one ratio.[55]

The binding constants of **7j**, **7n**, **7o**, **7r** and **7s** were calculated from the intercept as $8.04x10^5$, $7.25x10^5$, $4.35x10^3$, $3.13x10^3$ and $8.7x10^4$ M^{-1} which indicates strong binding of **7j**, **7n**, **7o**, **7r** and **7s** to AChE. Interestingly, there is a good correlation with the computationally calculated binding constants as $2.64x10^6$, $8.26x10^5$, $3.68x10^3$, $2.65x10^3$ and $1.12x10^5$ M^{-1} for **7j**, **7n**, **7o**, **7r** and **7s** obtained as the lowest free energy.

Figure 5 (here)

Free Energy Calculations

From the binding constants, the standard free energy change could be calculated according to the following equation.

$$\Delta G^\circ = -RT \ln K \qquad [3]$$

Where ΔG° is a free energy change, K is a binding constant and R is the gas constant at room temperature.

It is known that the binding constant obtained from the fluorescence emission data can also be used to predict binding interactions between small molecules (**7j**, **7n**, **7o**, **7r** and **7s**) and macro molecules (AChE), includes hydrogen bonds, van der Waals interactions, electrostatic forces, and hydrophobic interactions.[56] The signs and magnitudes of thermodynamic parameters are the main evidence for insisting the forces involved in the protein-drug binding and their stability. The negative values of ΔG° explain the nature of the reaction as exothermic and demonstrated the easy formation of **7j**, **7n**, **7o**, **7r** and **7s**-AChE complex. Thus the experimentally calculated

free energy changes are −7.32 kcal M^{-1}, −8.34 kcal M^{-1}, −7.96 kcal M^{-1}, −8.54 kcal M^{-1} and −6.78 kcal M^{-1} for **7j**, **7n**, **7o**, **7r** and **7s**, respectively. The negative value of the free energy of binding flavones derivatives to AChE is mainly due to hydrophobic interactions. This is further supported by the interactions and binding energy of AChE obtained from *in silico* calculations which were found to be −8.76 kcal M^{-1}, −8.07 kcal M^{-1}, −8.90 kcal M^{-1}, −8.70 kcal $M^{-1}$and −6.89 kcal $M^{-1}$for the lowest conformations of **7j**, **7n**, **7o**, **7r** and **7s** respectively. Similar types of interactions such as hydrophobic and hydrogen bonding were observed with our recent studies on natural as well as synthetic analogs with proteins. [51, 53, 55, 57] Also, our recent report on flavone derivatives revealed similar binding free energies as −5.4 Kcal M^{-1} for trimethoxy flavones.[57]

Secondary Structure analysis: Studied by Circular Dichroism

CD spectroscopy is the most vigorous analytical technique to understand the secondary and tertiary structural changes, conformation, and stability of proteins in solution.[58, 59] CD signal is observed for chromophores in proteins that are chiral either intrinsically due to its structure or when in asymmetric environments due to a 3-dimensional structure. Consequently, CD can give a very good estimation of the fraction of the residues such as α-helical, β-sheet and random coil in the protein structures and possibly their inter-conversions. Thus, to interpret the overall structural changes of AChE upon interaction with **7j**, **7n**, **7o**, **7r** and **7s** the CD experiments were carried out between 260 and approximately 190 nm at fixed concentration of AChE in the presence of different concentrations of **7j**, **7n**, **7o**, **7r** and **7s**. In the case of AChE, the CD spectra consist of two negative bands at 208 and 220 nm which are originated from α-helix in protein. [53, 57] Upon addition of **7j**, **7n**, **7o**, **7r** and **7s** to free AChE at various concentrations, the decrease in

intensity of bands at 208 and 222 nm in a concentration-dependent manner were noticed (Figure 6) & (Figure S4 in Supplementary Information), which indicated a decrease in the α-helix with an increase in the β-sheets and random coils. The secondary structure of free AChE consists of ~30.61% α-helix, ~17.07% β-sheets and ~52.32% random coils, which is in agreement with previous reports.[60] Conformational analysis by web based software CDNN 2.1 revealed that at high concentrations there were apparent changes in the secondary structure of the protein as follows: **7j**: α-helix; 32.62 ± 1.65 to 30.52 ± 1.10: β-sheets; 17.38 ± 0.45 to 17.58 ± 0.5: Random Coil; 49.78 ± 2.16 to 52.42 ± 2.79. **7n**: α-helix; 30.75 ± 1.51 to 23.49 ± 1.16: β-sheets; 17.37 ± 0.49 to 17.98 ± 0.75: Random coil; 51.54 ± 2.25 to 58.63 ± 2.67. **7o**: α-helix; 30.76 ± 1.16 to 26.43 ± 0.96: β-sheets; 17.38 ± 0.56 to 17.79 ± 0.81: Random coil; 51.93 ± 2.16 to 55.90 ± 2.46. **7r**: α-helix; 30.10 ± 0.90 to 26.82 ± 1.25: β-sheets; 17.37 ± 0.32 to 17.60 ± 0.45: Random coil; 52.30 ± 2.35 to 55.58 ± 2.25. **7s**: α-helix; 30.74 ± 0.89 to 26.90 ± 1.15: β-sheets; 17.21 ± 0.54 to 17.58 ± 0.39: Random coil; 51.92 ± 2.41 to 55.45 ± 2.38 (see Table S1 in Supplementary Information). The decrease of α-helix and increase of β-helix and random coils is in the order of **7n**> **7o**> **7s**> **7r**> **7j**. The decrease in the α-helix accompanied with the increase in the β-sheets and random coils indicated the partial unfolding of second structure of AChE with flavones analogues, suggesting the formation of **7j**, **7n**, **7o**, **7r** and **7s**- AChE complexes.

This partial unfolding may be due to change in microenvironment within the proximity of tryptophan residue while binding to flavone analogs, which was also very well supported by fluorescence studies. Similar studies on change in protein conformation upon binding of different drug molecules were reported by our group. [51, 53, 55, 57]

Figure 6 (here)

Molecular Docking Studies

The molecular docking, an important computational procedure has been employed to understand the interaction and also to confirm the binding site of drugs on the protein, since the knowledge on the binding location of a biologically active drug within the protein environment is a crucial prerequisite to explain its therapeutic efficacy.

The X-ray crystallographic structure analysis of AChE has provided insights into the essential structural elements and motifs central to its catalytic mechanism and mode of Ach processing.[61, 62] One of the striking structural features is that AChE consists of a narrow, long, hydrophobic gorge, which is approximately 20 Å deep.[63] The X-ray crystallographic structure of AChE revealed three main binding sites. The catalytic anionic site (CAS) comprising Ser203, Glu334, and His447 as catalytic triad at the bottom of active site interacts with the cationic substrates, for example ACh.[64] The anionic binding site near the CAS consisting of Trp84, Tyr130, Glu199, His441, His444, and Tyr337 at the vicinity of the catalytic triad interacts with quaternary ammonium functionality of many ligands. Additionally, there is a peripheral anionic site (PAS) composed of Tyr72, Asp74, Tyr124, and Trp286, which located at the gorge entrance.[65] Furthermore, the key residue Phe330 in the mid gorge is also involved in the recognition of ligands. Recent studies have demonstrated that the PAS might accelerate the aggregation and deposition of β-amyloid peptide, which are considered as another cause of AD.[66]

In this study, 3D structure of *Ee*AChE 1C2O (from *Electric eel*) (enzyme species was used for the *in vitro* experiments) was retrieved from Brookhaven Protein Data Bank for docking purposes. To predict the binding site and types of interactions involved in the formation of **7j**, **7n**, **7o**, **7r** and **7**- AChE complexes, molecular docking was performed using Lamarckian genetic algorithm implemented in Autodock 4.2.3. Among 30 conformations generated from docking simulation, only one conformer with the least binding free energy and score ranking that match

with fluorescence emission data was selected for further analysis.[67] Docking results deciphers that **7j**, **7n**, **7o**, **7r** and **7s** are binding to AChE at PAS region within the vicinity of the active site (Figure 7 & 8 and figure S5 & S6 in Supplementary Information).

The docking results indicated that among the flavones derivatives, **7j** is bound to the PAS surrounded by Phe295, Trp286, Tyr124 and Phe297, **7n** surrounded by Gln291, Trp286, Tyr124, Asp74, Thr83 and Tyr341, **7o** enclosed towards Trp286, Tyr124, Phe297, Phe295, amino acids like Ser 293, Phe295, Phe297, Tyr341 surrounds the **7s** and compound **7o** encircled with Trp286, Tyr124, Phe295 and Phe297. It is also observed that among the five analogues only **7o** was stabilized completely by hydrophobic interactions whereas **7j**, **7n**, **7r** and **7s** had one hydrogen bonding interaction with hydrophilic amino acids in the gorge. The **7j** –AChE complex is stabilized by hydrogen bond between NH group of Phe295 and C=O group of C ring in the compound with the bond length of 1.982 Å. **7n** –AChE complex is stabilized by a hydrogen bond between the amide group of **7n** and the carboxylic group of Gln291 amino acid residue of the AChE with length of 2.22 Å, **7r** derivative-AChE complex by a hydrogen bond between the amide group of compound and phenolic OH group of Tyr72 with the bond length of 2.088 Å and NH group of Ser293 complex by a hydrogen bond with amide group of **7s** with bond length 1.655 Å.

The computationally calculated binding energies of the lowest energy conformers of the **7j**, **7n**, **7o**, **7r** and **7s** derivatives are −8.76 Kcal/mol, −8.07 Kcal/mol, −8.9 Kcal/mol, −8.7 Kcal/mol and −6.89 Kcal/mol, respectively which are close to the experimentally calculated free energies derived from fluorescence data −7.32, −8.34, −7.96, −8.54 and −6.78 Kcal/mol for **7j**, **7n**, **7o**, **7r** and **7s** derivatives, respectively, at 25 °C. Fascinatingly molecular docking studies revealed that these **7j**, **7n**, **7o**, **7r** and **7s** derivatives showed the interactions with AChE with binding constants

2.64 x 10^6, 8.26 x 10^5, 3.68 x 10^3, 2.65 x 10^3 and 1.12 x 10^5 M^{-1}. Furthermore these values seem to be close to experimental binding constant values 8.04 x 10^5, 7.25 x 10^5, 4.35 x 10^3, 3.13 x 10^3 and 8.7 x 10^4 M^{-1} respectively suggesting that these analogues are strong enough to bind with AChE, which is important for their therapeutic action against AD.

Figure 7 and **8** (here)

CONCLUSIONS

In conclusion, in this study, a novel series of flavone-cyanoacetamide related compounds **7a-s** with a multifunctional profile is reported. Among the series of the novel chemical entities assayed, **7j**, **7n**, **7o**, **7r** and **7s** were characterized as AChE inhibitors of submicromolar potency and also highly selective for AChE over BuChE. Kinetic analysis of AChE inhibition and the auto docking studies indicated that compound **7s** showed mixed-type inhibition and could bind to PAS in such a way that compound protrude out from the gorge of AChE. Furthermore, **7i** and **7j** **7e**, **7n**, **7p,** **7k**, **7o**, **7q** and **7r** were also endowed with some antioxidant properties through ABTS radical scavenging abilities in the IC_{50} range of 16.24 to 49.84 μM. Additionally, **7j**, **7n**, **7o**, **7r** and **7s** conceived for accelerating the aggregation of Aβ peptide to convert the Aβ monomers and oligomers into aggregates and alleviate the Aβ-induced toxicity, since oligomers accounted to be more toxic forms to neurons in comparison with the fibril aggregates. The cell viability results depicted that the compounds **7j**, **7r** and **7s** were nontoxic to SK-N-SH cells at lower (40 μM) concentrations. Amongst the tested **7r** is nontoxic to SK-N-SH cells similar to that of galantamine and had extremely high protective activities at all the concentrations. Compounds **7j**, **7r** and **7s** also exhibited significant neuroprotective effects at low concentrations

(40 and 80 μM) in human SK-N-SH neuroblastoma cells against oxidative stress-associated death induced by H_2O_2. Later, binding constants and free energy values obtained from fluorescence studies showed that flavones derivatives quenched AChE intrinsic fluorescence via static quenching mode and the binding processes were spontaneous mainly through hydrophobic interactions. Conformational analysis revealed that the protein secondary structure is changed, so that α-helical content of AChE with flavones analogs decreased with consequent increase in the β -sheets and random coils which indicates partial unfolding of the protein. Binding site analysis by docking study validated that flavone analogues bound to PAS binding site with hydrophobic and hydrogen bonding interactions. Taken together, these findings will pave the way to the development of flavone and cyanoacetamide hybrids as novel multifunctional anti-Alzheimer's candidates worthy of additional *in vivo* studies.

ASSOCIATED CONTENT

Supporting Information available

Supporting Information consists of copies of NMR spectra of the synthesized compounds, detection of Aβ aggregates of **7r** and **7s** using ThT assay, fluorescence emission spectra for **7r** and **7s** , Plot of log (Fo/F) against [Q] of **7j**, **7n**, **7o**, **7r** and **7s**-AChE, Circular dichorism (CD) spectra of AChE and its complexes with **7r** and 7s, docking figures of **7r** and **7s** and a table with Percentage of **s**econdary structure of AChE and AChE-**7j**, **7n**, **7o**, **7r** and **7s** complex.

This material is available free of charge on the ACS Publications website.

AUTHOR INFORMATION

Corresponding author

Prof. Amooru Gangaiah Damu, Department of Chemistry, Yogi Vemana University, Kadapa-516003, Andhra Pradesh, India. Phone: +91-8562-225410 (Off.), +91-9177888961 (Mobile); Fax: +91-8562-225419; e-mail: agdamu01@gmail.com.

ORCID

Amooru Gangaiah Damu: 0000-0002-6578-3232

Author Contributions

This manuscript was made through the contribution of all authors. All authors were given approval to the final version of the manuscript.

ACKNOWLEDGEMENT

This work was supported through (SR/FT/CS-60/2010) from Department of Science and Technology (DST) and a grant under Empowerment and Equity Opportunity for Excellence in Science program from Science and Engineering Board (SB/EMEQ-155/2013), DST, New Delhi, India. The authors are also grateful to Dr. V. Ramakrishna, Assistant Professor, Yogi Vemana University, for the valuable suggestions extended towards the cell viability, neuroprotectivity and antioxidant studies. The authors thank Department of Chemistry, Pondicherry University for providing ESI HRMS spectra from DST FIST facility and Dr. K.S.V. Krishna Rao for providing IR instrumental facility.

ABBREVIATIONS

AD, Alzheimer disease; CNS, central nervous system; Ach, acetylcholine; AChE, Acetylcholinesterase; BuChE, Butyrylcholinesterase; Aβ, amyloid beta; ROS, reactive oxygen species; MTLDs, multi-target directed ligands; HMTA, hexamethylenetetramine; *E*AChE Acetylcholinesterase from *Electrophorus electricus*; ABTS, 2,2'-azino-bis(3-ethylbenzthiazoline-6-sulfonic acid); ThT, thioflavin T; CD, circular dichroism; CAS, catalytic anionic site; PAS, peripheral anionic site; TLC, thin-layer chromatography; NMR, nuclear magnetic resonance; TMS, tetramethylsilane; MW, micro wave; HRMS, high resolution mass spectroscometry; ChE, cholinesterases; DTNB, 5,5'-dithio-bis(2-nitrobenzoic acid); ATCh, acetylthiocholine iodide; BTCh, butyrylthiocholine iodide; DMSO, dimethylsulfoxide; Rpm, resolutions per minute; PBS, phosphate buffer saline; NCCS, National centre for cell sciences; MEM, minimal essential medium; FBS, fetal bovine serum; LGA, Lamarckian genetic algorithm; PDB, protein data bank.

REFERENCES

(1) Walsh, D. M.; Selkoe, D. J. Deciphering the molecular basis of memory failure in Alzheimer's disease. *Neuron*. **2004**, *44*, 181–193.

(2) Alzheimer's Association. Alzheimer's Disease facts and figures. *Alzheimers Dement*. **2017**, *13*, 325–373.

(3) Yan, H.; Pei-Fen, Y.; Shuo-bin, C.; Zhi-hong, H.; Shi-Liang, H.; Jia-Heng, T.; Ding, L.; Lian-Quan, G.; Zhi-Shu, H. Synthesis and evaluation of 7,8-dehydrorutaecarpine derivatives as potential multifunctional agents for the treatment of Alzheimer's disease. *Eur. J. Med. Chem*. **2013**, *63*, 299–312.

(4) Maria, D.; Begona, O.; Alejandro, S.; Juan-Antonio, M.; Inmaculada, F. A review of chronic pain impact on patients, their social environment and the health care system. *J. Pain Res.* **2016**, *9*, 457–467.

(5) Corbett, A.; Pickett, J.; Burns, A.; Corcoran, J.; Dunnett, S. B.; Edison, P.; Hagan, J. J.; Holmes, C.; Jones, E.; Katona, C.; Kearns, I.; Kehoe, P.; Mudher, A.; Passmore, A.; Shepherd, N.; Walsh, F.; Ballard, C. Drug repositioning for Alzheimer's disease. *Nat. Rev. Drug Discov*. **2012**, *11*, 833–846.

(6) Shixian, L.; Hui, D.; Shengbin, H.; Jingyuan, Y.; Siqian, W.; Baodi, Y.; Tieli, Z.; Dafeng, Z.; Jinsong, L.; Guohui, G.; Jianfeng, M.; Zhennan, D. Design, synthesis and evaluation of novel 5,6,7-trimethoxyflavone–6-chlorotacrine hybrids as potential multifunctional agents for the treatment of Alzheimer's disease. *Bioorg. Med. Chem. Lett.* **2015**, *25*, 1541–1545.

(7) Atwood, C. S.; Robinson, S. R.; Smith, M. A. Amyloid-beta: redox-metal chelator and antioxidant. *J. Alzheimers Dis.* **2002**, *4*, 203–214.

(8) Pacheco, G.; Palacios-Esquivel, R.; Moss, D. E. Cholinesterase inhibitors proposed for treating dementia in Alzheimer's disease: selectivity toward human brain acetylcholinesterase compared with butyrylcholinesterase. *J. Pharmacol. Exp. Ther*. **1995**, *274*, 767–770.

(9) Liston, D. R.; Nielsen, J. A.; Villalobos, A.; Chapin, D.; Jones, S. B.; Hubbard, S. T.; Shalaby, I. A.; Ramirez, A.; Nason, D.; White, W. F. Pharmacology of selective acetylcholinesterase inhibitors: implications for use in Alzheimer's disease. *Eur. J. Pharmacol*. **2004**, *486*, 9–17.

(10) Hamley, I. W. The amyloid beta peptide: A chemist's perspective. Role in Alzheimer's and fibrillization. *Chem. Rev*. **2012**, *112*, 5147–5192.

(11) Selkoe, D. J. Translating cell biology into therapeutic advances in Alzheimer's disease. *Nature*. **1999**, *399*, A23–A31.

(12) Bucciantini, M.; Giannoni, E.; Chiti, F.; Baroni, F.; Formigli, L.; Zurdo, J. S.; Taddei, N.; Ramponi, G.; Dobson, C. M.; Stefani, M. Inherent toxicity of aggregates implies a common mechanism for protein misfolding diseases. *Nature*. **2002**, *416*, 507–511.

(13) Selkoe, D. J. Folding Proteins in Fatal Ways. *Nature*, **2003**,*426*, 900–904.

(14) Klein, W. L. A-beta toxicity in Alzheimer's disease: Globular oligomers (ADDLs) as new vaccine and drug targets. *Neu. chem. Int*. **2002**, *41*, 345–352.

(15) McLaurin, J.; Yang, D. S.; Yip, C. M.; Fraser P. E. Review: Modulating factors in Amyloid-β fibril formation. *Journal of Structural Biology*. **2000,** *130*, 259–270.

(16) Giunta, B.; Fernandez, F.; Nikolic, W. V.; Obregon, D.; Rrapo, E.; Town, T.; Tan, J. Inflammaging as a prodrome to Alzheimer's disease. *Neuroinflammation.* **2008**, *5*, 51.

(17) Thiratmatrakul, S.; Yenjai, C.; Waiwut, P.; Vajragupta, O.; Reubroycharoen, P.; Tohda, M.; Boonyarat, C. Synthesis, biological evaluation and molecular modeling study of novel Tacrine-carbazole hybrids as potential multifunctional agents for the treatment of Alzheimer's disease. *Eur. J. Med. Chem*. **2014**, *75*, 21–30.

(18) Lu, C.; Guo, Y.; Yan, J.; Luo, Z.; Luo, H. B.; Yan, M.; Huang, L.; Li, X. Design, synthesis, and evaluation of multitarget-directed resveratrol derivatives for the treatment of Alzheimer's disease. *J. Med. Chem.* **2013**, *56*, 5843–5859.

(19) Sun, Q.; Peng, D. Y.; Yang, S. G.; Zhu, X. L.; Yang, W. C.; Yang, G. F. Syntheses of coumarin-tacrine hybrids as dual-site acetylcholinesterase inhibitors and their activity against butylcholinesterase, Aβ aggregation, and β-secretase. *Bioorg. Med. Chem.* **2014**, *22*, 4784–4791.

(20) Diasa, K. S. T.; Jr, C. V. Multi-Target Directed Drugs: A Modern Approach for Design of New Drugs for the treatment of Alzheimer's disease. *Current Neuropharmacology*. **2014**, *12*, 239–255.

(21) Basha, S. J.; Kumar, P. B.; Mohan, P.; Viswanath, K. K.; Subba Rao, D.; Siddhartha, E.; Manidhar, D. M.; Dinakara Rao, A.; Ramakrishna, V.; Damu, **A**. G. Synthesis, pharmacological assessment, molecular modeling and in silico studies of fused tricyclic coumarin derivatives as a new family of multifunctional anti-Alzheimer agents. *Eur. J. Med. Chem*. **2016**, *107*, 219–232.

(22) Basha, S .J.; Kumar, P. B.; Mohan, P.; Siddhartha, E.; Manidhar, D. M.; Rao, A. D.; Ramakrishna, V.; Damu, A. G. Synthesis, biological evaluation and molecular docking *of 8-imino-2-oxo-2H,8H-pyrano[2,3-f] chromene* analogues: New dual AChE inhibitors as potential drugs for the treatment of Alzheimer's disease. *Chemical Biology & Drug Design*. **2016**, *88*, 43–53.

(23) Jung, M.; Park, M. Acetylcholinesterase inhibition by flavonoids from *Agrimonia pilosa*. *Molecules.* **2007**, *12*, 2130–2139.

(24) Kim, J. Y.; Lee, W. S.; Kim, Y. S.; Curtis-Long, M. J.; Lee, B. W.; Ryu, Y. B.; Park, K. H. Isolation of cholinesterase-inhibiting flavonoids from *Morus lhou. Journal of Agriculture and Food Chemistry*. **2011**, *59*, 4589–4596.

(25) Rostom, S.; El-Ashmawy, I. M.; Abd El Razik, H. A.; Badr, M. H.; Ashour, H. M. A. Design and synthesis of some thiazolyl and thiadiazolyl derivatives of antipyrine as potential non-acidic anti-inflammatory, analgesic and antimicrobial agents. *Bioorg*. *Med. Chem*. **2009**, *17*, 882–895.

(26) Busch, B. B.; Stevens Jr, W. C.; Martin, R.; Ordentlich, P.; Zhou, S.; Sapp, D. W.; Horlick, R. A.; Mohan, R. Identification of a selective inverse agonist for the orphan nuclear receptor estrogen-related receptor alpha. *J. Med. Chem.* **2004**, *47*, 5593–5596.

(27) Murthy, Y. L. N.; Kasiviswanath, I. V.; Nageswarpandit, E. Synthesis, characterization & antibacterial activity of 7, 4' – Dihydroxy, 3'-methoxy flavones. *Int. J. Chem Tech Res.* **2010**, *2*, 1097–1101.

(28) Cooper, S. R.; Drake, N. L.; Anspon, H. D.; Mozingo, R. Resacetophenone, *Organic Synthesis.* **1955**, *3*, 761.

(29) Baker, W. Molecular Rearrangement of Some o-Acyhxyacetophenonesan the mechanism of the production of 3-Acylchromones. *J. Chem. Soc.* **1933**, 1381–1389.

(30) X-ping, L.; Ying, W.; H-yu, L.; A-hua, S.; K-keung, T.; T-xia D.; Chun, H.; Synthesis and anti-inflammatory activity of a novel series of 9,10-Dihydro-4*H*,8*H*-chromeno[8,7-e][1,3]oxazin-4-one Derivatives. *Chem. Res. Chinese Universities.* **2010**, *26*, 268–271.

(31) Tang, L. J.; Zhang, S. F.; Yang, J. Z. *Org. Prep. Proced. Int.* **2004**, *36*, 453.

(32) Panel, A. D.; Sangita, S.; Vorz, J. J.; Joshi, J. D. Synthesis, characterisation and antimicrobial activities of binary and ternary complexes of $UO_2^{II}$and Th^{IV} complexes with 5-hydroxymethyl-8-quinolinol and 8-formyl-7-hydroxy-4-methyl- 2H-1-benzopyran-2-one with aniline. *J. Indian Chem. Soc.* **1997**, *74*, 287–288.

(33) Volmajer, J.; Toplak, R.; Lebanb, I.; Le Marechala, A. M. Synthesis of new imino coumarins and their transformations into N-chloro and hydrazono compounds. *Tetrahedron.* **2005**, *61*, 7012–7021.

(34) Ellman, G. L.; Courtney, K. D.; Andres Jr, V.; Featherstone, R. M. A new and rapid colorimetric determination of acetylcholinesterase activity. *Biochem. Pharmacol*. **1961**, *7*, 88–95.

(35) Nadri, H.; Pirali-Hamedani, M.; Shekarchi, M.; Abdollahi, M.; Sheibani, V.; M. Amanlou, M. Design, synthesis and anticholinesterase activity of a novel series of 1-benzyl-4-((6-alkoxy-3-oxobenzofuran-2(3H)-ylidene) methyl) pyridinium derivatives. *Bioorg. Med. Chem*. **2010**, *18*, 6360–6366.

(36) Rampa, A.; Bisi, F.; Belluti, S.; Gobbi, P.; Valenti, V.; Andrisano, V.; Cavrini, A.; Cavalli, M.; Acetylcholinesterase inhibitors for potential use in Alzheimer's disease: molecular modeling, synthesis and kinetic evaluation of 11H-indeno-[1,2-b]-quinolin-10-ylamine derivatives, *Bioorg. Med. Chem.* **2000**, *8*, 497–506.

(37) Miller, N. J.; Rice-Evans, C. A. Factors influencing the antioxidant activity determined by the $ABTS^{\cdot+}$ radical cation assay. *Free Radic. Res*. **1997**, *26*, 195–199.

(38) Fang L.; Fang X.; Gou S.; Lupp A.; Lenhardt I.; Sun Y.; Huang Z.; Chen Y.; Zhang Y.; Fleck C. Design, synthesis and biological evaluation of D-ring opened galantamine analogs as multifunctional anti- Alzheimer agents. *Eur. J. Med. Chem*. **2014**, *76*, 376–386.

(39) Ramakrishna, V.; Preeti Gupta, K.; OrugantiSetty, H.; Anand, K.; Neuroprotective effect of *Emblica officinalis* extract against H_2O_2 induced DNA damage and repair in neuroblastoma cells. *J. Homeop. Ayurv. Med.* **2014**, *1002*, 1–5.

(40) Daniel, P. Y.; Mahesh, G.; Manidhar, D. M.; Aparna, R.; Sailaja, N.; Suresh Reddy, C.; Rajagopal, S. Binding and Molecular Dynamics Studies of 7-Hydroxycoumarin Derivatives with Human Serum Albumin and its Pharmacological Importance. *Molecular Pharmaceutics.* **2014**, *11*, 1117–1131.

(41) Mahesh, G.; Narayana, V. V.; Vineet, S.; Shatabdi, R. C.; Sreelaxmi, V.; Ramachary, D. B.; Rajagopal S. Unravelling the Binding Mechanism and Protein Stability of Human Serum Albumin while Interacting with Nefopam Analogues: A Biophysical and Insilco approach. *Journal of Biomolecular Structure and Dynamics.* **2017**, *35*, 2280–2292.

(42) Daniel, P. Y.; Aparna, R.; Rajagopal, S. A comparative binding mechanism between human serum albumin and α-1-acid glycoprotein with corilagin: biophysical and computational approach. *RSC Adv.* **2016**, *6*, 40225–40237.

(43) Sudhamalla, B.; Gokara, M.; Ahalawat, N.; Amooru, D. G.; Subramanyam, R. Molecular dynamics simulation and binding studies of β-sitosterol with human serum albumin and its biological relevance. *The Journal of Physical Chemistry B.* **2010**, *114*, 9054–9062.

(44) Morris, G. M.; Huey, R.; Lindstrom, W.; Sanner, M. F.; Belew, R. K.; Goodsell, D. S.; Olson, A. J. AutoDock 4 and AutoDock Tools 4: Automated docking with selective receptor flexibility. *Journal of computational chemistry.* **2009**, *30*, 2785–2791.

(45) Malleda, C.; Ahalawat, N.; Gokara, M.; Subramanyam, R. Molecular dynamics simulation studies of betulinic acid with human serum albumin. *Journal of Molecular Modeling.* **2012**, *18*, 2589–2597.

(46) Wu¨rthner, F.; Thalacker, C.; Sautter, A. Hierarchical Organization of Functional Perylene Chromophores to Mesoscopic Superstructures by Hydrogen Bonding and $\pi-\pi$ Interactions. *Adv. Mater.* **1999**, *11*, 754–758.

(47) Hirschberg, J. H. K. K.; Brunsveld, L.; Ramzi, A.; Vekemans, J. A. J. M.; Sijbesma, R. P.; Meijer, E. W. Helical Self-Assembled Polymers from Cooperative Stacking of Hydrogen-Bonding Pairs. *Nature.* **2000**, *407*, 167–170.

(48) Balakrishnan M.; Chowdhury S. R.; Parameswar K. I. Modulation of amyloid‑β fibrils into mature microrod-shaped structure by histidine functionalized water-soluble perylene diimide *ACS Appl. Mater. Interfaces*. **2015**, *7*, 21226–21234.

(49) Bucciantini, M.; Giannoni, E.; Chiti, F.; Baroni, F.; Formigli, L.; Zurdo, J. S.; Taddei, N.; Ramponi, G.; Dobson, C. M.; Stefani, M. Inherent toxicity of aggregates implies a common mechanism for protein misfolding diseases. *Nature*. **2002**, *416*, 507–511.

(50) Lakowicz, J. R. Principles of fluorescence spectroscopy. *Berlin: Springer.* **2006**, *8*, 278–292.

(51) Mahesh G.; Tirupathi M.; Suresh K. K.; Reddanna P.; Rajagopal S. Unraveling the binding mechanism of asiatic acid with human serum albumin and its biological implications. *Journal of Biomolecular Structure and Dynamics*. **2013**, *32*, 1290–1302.

(52) Agudelo, D.; Bourassa, P.; Bruneau, J.; Bérubé, G.; Asselin, É.; Tajmir-Riahi, H. A. Probing the binding sites of antibiotic drugs doxorubicin and N-(trifluoroacetyl) doxorubicin with human and bovine serum albumins. *PLoS ONE*. **2012**, *7*, e43814.

(53) Neelam, S.; Gokara, M.; Sudhamalla, B.; Amooru D. G.; Subramanyam, R. Interaction Studies of Coumaroyltyramine with Human Serum Albumin and Its Biological Importance. *The Journal of Physical Chemistry B*. **2010**, *114*, 3005–3012.

(54) Min, J.; Meng-Xia, X.; Dong, Z.; Yuan, L.; Xiao-Yu L.; Xing, C. Spectroscopic studies on the interaction of cinnamic acid and its hydroxyl derivatives with human serum albumin. *Journal of Molecular Structure*. **2004**, *692*, 71–80.

(55) Yeggoni, D. P. R.; Darla, M. M.; Reddy C. S.; Subramanyam R. Investigation of binding mechanism of novel 8-substituted coumarin derivatives with human serum albumin and α-1-glycoprotein. *Journal of Biomolecular Structure and Dynamics.* **2016**, *34*, 2023–2036.

(56) Leckband, D. Measuring the forces that control protein interactions. *Annual Review of Biophysics and Biomolecular Structure*. **2000**, *29*, 1–26.

(57) Gokara, M.; Sudhamalla, B.; Amooru, D. G.; Subramanyam, R. Molecular interaction studies of trimethoxy flavone with human serum albumin. *PLoS One.* **2010**, *5*, e8834.

(58) Gray, D. M.; Hung, S. H.; Johnson, K. H. Absorption and circular dichroism spectroscopy of nucleic acid duplexes and triplexes. *Methods in Enzymology*. **1995**, 246, 19–34.

(59) Sun, C.; Yang, J.; Wu, X.; Huang, X.; Wang, F.; Liu, S. Unfolding and refolding of bovine serum albumin induced by cetylpyridinium bromide. *Biophysical Journal*. **2005**, *88*, 3518–3524.

(60) Garnier, J.; Gibrat, J. F.; Robson, B. GOR secondary structure prediction method version IV, *Methods in Enzymology.* **1996**, *266*, 540–553.

(61) Harel, M.; Quinn, D. M.; Nair, H. K.; Silman, I.; Sussman, J. L. The X-ray structure of a transition state analog complex reveals the molecular origins of the catalytic power and substrate specificity of acetylcholinesterase. *J. Am. Chem. Soc.* **1996**, *118*, 2340–2346.

(62) Greenblatt, H. M.; Kryger, G.; Lewis, T.; Silman, I.; Sussman, J. L. Structure of acetylcholinesterase complexed with (-)-galanthamine at 2.3 A resolution. *FEBS Lett*. **1999**, *463*, 321–326.

(63) Botti, S. A.; Felder, C. E.; Lifson, S.; Sussman, J. L.; Silman, I. A modular treatment of molecular traffic through the active site of cholinesterase. *Bio. phys. J*. **1999**, *77*, 2430–2450.

(64) Ordentlich, A.; Barak, D.; Kronman, C.; Flashner, Y.; Leitner, M.; Segall, Y.; Ariel, N.; Cohen, S.; Velan, B.; Shafferman, A. Dissection of the human acetylcholinesterase active center determinants of substrate specificity. Identification of residues constituting the anionic site, the hydrophobic site, and the acyl pocket. *J. Biol. Chem*. **1993**, *268*, 17083–17095.

(65) Barak, D.; Kronman, C.; Ordentlich, A.; Ariel, N.; Bromberg, A.; Marcus, D.; Lazar, A.; Velan, B.; Shafferman, A. Acetylcholinesterase peripheral anionic site degeneracy conferred by amino acid arrays sharing a common core. *J. Biol. Chem.* **1994**, *269*, 6296–6305.

(66) De Ferrari, G. V.; Canales, M. A.; Shin, I.; Weiner, L. M.; Silman, I.; Inestrosa, N. C. A structural motif of acetylcholinesterase that promotes amyloid beta-peptide fibril formation. *Biochemistry.* **2001**, *40*, 10447–10457.

(67) Jones, G.; Willett, P.; Glen, R. C.; Leach, A. R.; Taylor, R. Development and validation of a genetic algorithm for flexible docking. *J. Mol. Biol.* **1997**, *267*, 727–748.

Figure legends:

Figure1. (a) Lineweaver Burk plot of AChE (0.4 U/mL) with substrate acetylthiocholineiodide (0.1-0.5 mM of concentration) in the absence and in presence of different concentrations of **7s** at 0.1, 0.4 and 1 μM. (b) Secondary plots of the Lineweaver–Burk plot of **7s**; slope versus various concentrations. (c) Intercept versus various concentrations.

Figure 2. Detection of Aβ aggregates using ThT assay; fluorescence enhancement spectra (λ_{ex} = 390 nm, λ_{em} = 450 nm) of ThT solution mixed with $A\beta_{1-42}$ different concentrations of (a) galantamine and test compounds (b) **7j**, (c) **7n**, and (d) **7o** measured after 24 h of incubation. In each panel, the independent experiments were performed thrice and each time identical spectra were obtained.

Figure 3. Neurotoxic effects of **7j**, **7n**, **7o**, **7r** and **7s** compounds on SK-N-SH cells (human neuroblastoma cell line). Bar chart shows the percentage of cell viability in the presence or absence (control) of indicated concentrations of **7j**, **7n**, **7o**, **7r**, **7s** and Galantamine. Three self-determining experiments were carried out and mean ± S.E.M was calculated and reported as (%)

of cell viability vs concentration (μM). *P < 0.05 versus 100% cell viability (one-way ANOVA test).

Figure 4. Neuroprotective activity of compounds **7j**, **7n**, **7o**, **7r**, **7s** galantamine and catechin against H_2O_2 induced cell death in SK-N-SH cells. *P < 0.05 versus H_2O_2 treatment.

Figure 5. Room temperature fluorescence emission spectra of flavone derivatives (a) **7j**, (b) **7n**, (c) **7o** and (d) **7r**. Inserts: Modified Stern-Volmer plots. Fluorescence emission spectra of ((a) **7j**, (b) **7n,** (c) **7o** and (d) **7r)** -AChE. Plot of log(dF/F) against log [Q] λex = 285 nm, λem = 360 nm.

Figure 6. Circular dichorism (CD) spectra of AChE and its complexes with flavone derivatives (a) **7j**, (b) **7n**, (c) **7o** and (d) **7r** were recorded with a JASCO J-1500 CD spectrometer. A quartz cell with a path length of 0.1cm was used. Inserts: Secondary structural elements of AChE and AChE plus **7j**, **7n, 7o** and **7r** derivatives, the plot shows concentration dependent secondary structural changes of free AChE, the AChE-**7j**, **7n, 7o** and **7r** complexes. The data were analyzed using the web based software CDNN 2.1.

Figure 7. Target compounds (a) **7j**, (b) **7n**, (c) **7r** and (d) **7s** were docked in the binding pocket of AChE using Autodock4.2.3. Target compounds were depicted in a ball and stick model (blue, grey, red and white), and AChE correspond in a line model.

Figure 8. Docking pose of (a) **7j**, (b) **7n**, (c) **7r** and (d) **7s** were at the outer side rim of the gorge of AChE (PAS). The images were generated using PyMol.

Figure1.

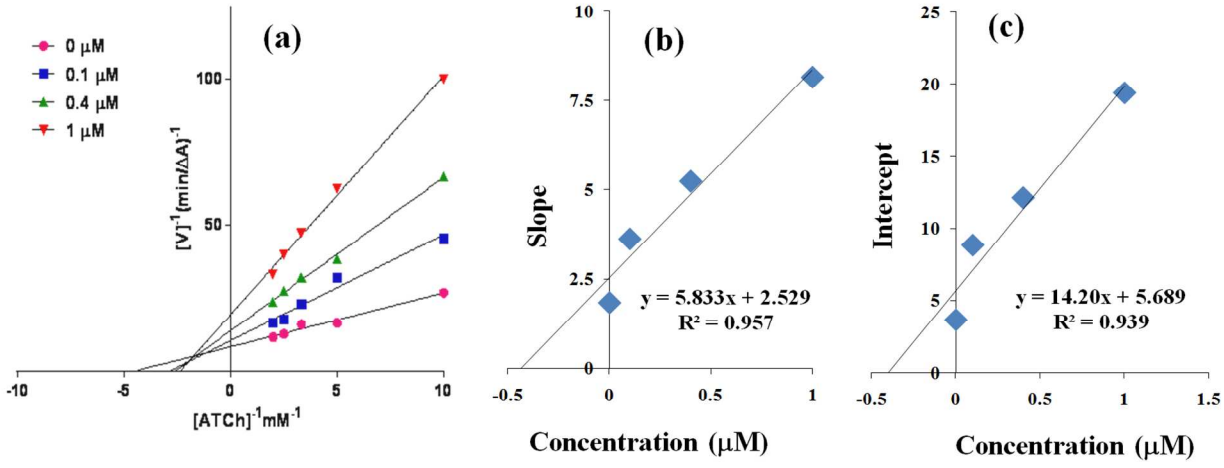
(a)
0 μM
0.1 μM
0.4 μM
1 μM
[V]-1 (min/ΔA)-1
[ATCh]-1mM-1
(b)
Slope
y = 5.833x + 2.529
R² = 0.957
Concentration (μM)
(c)
Intercept
y = 14.20x + 5.689
R² = 0.939
Concentration (μM)

Figure 2.

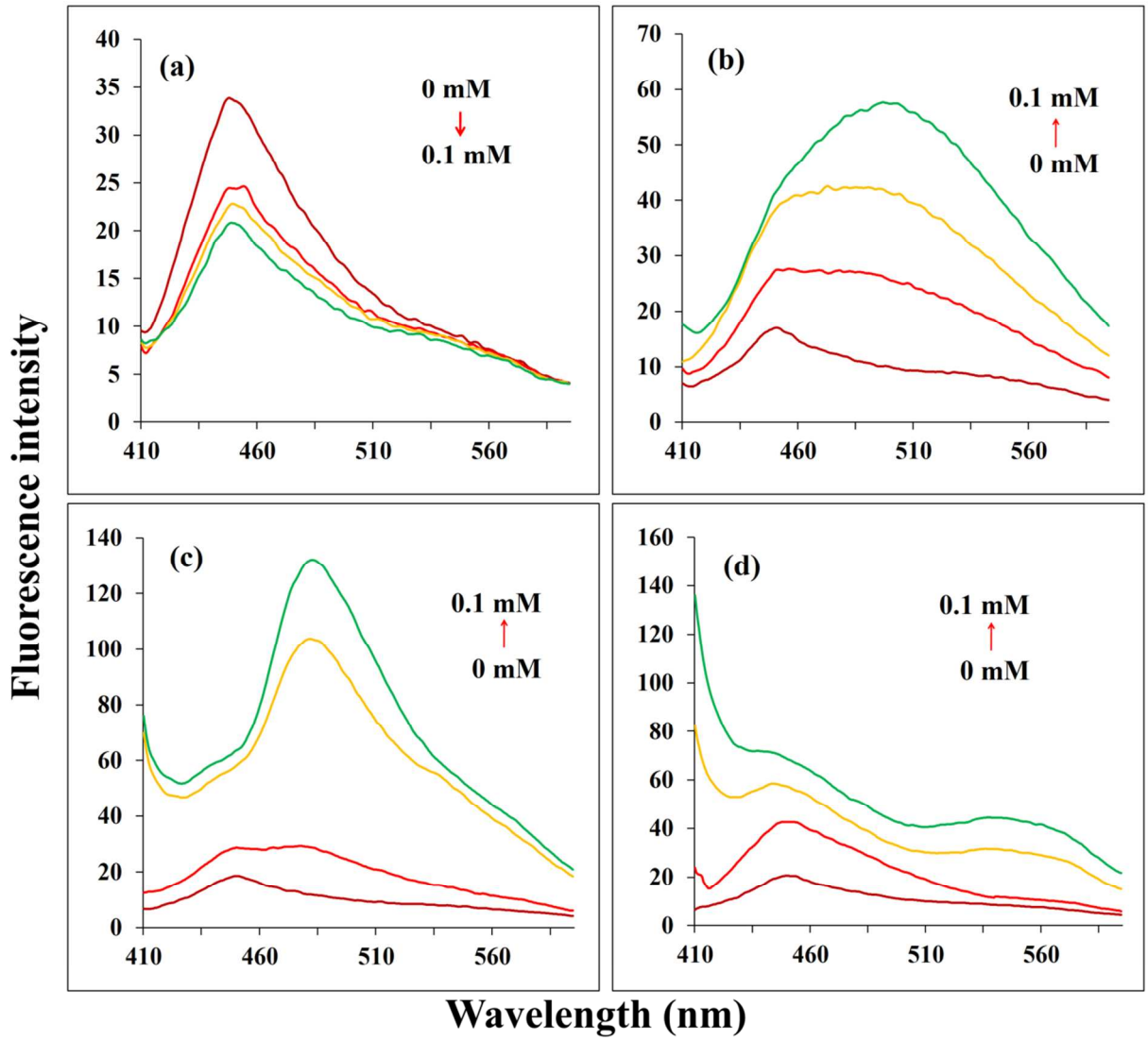
(a)
0 mM
0.1 mM
(b)
0.1 mM
0 mM
(c)
0.1 mM
0 mM
(d)
0.1 mM
0 mM
Fluorescence intensity
Wavelength (nm)

Figure 3.

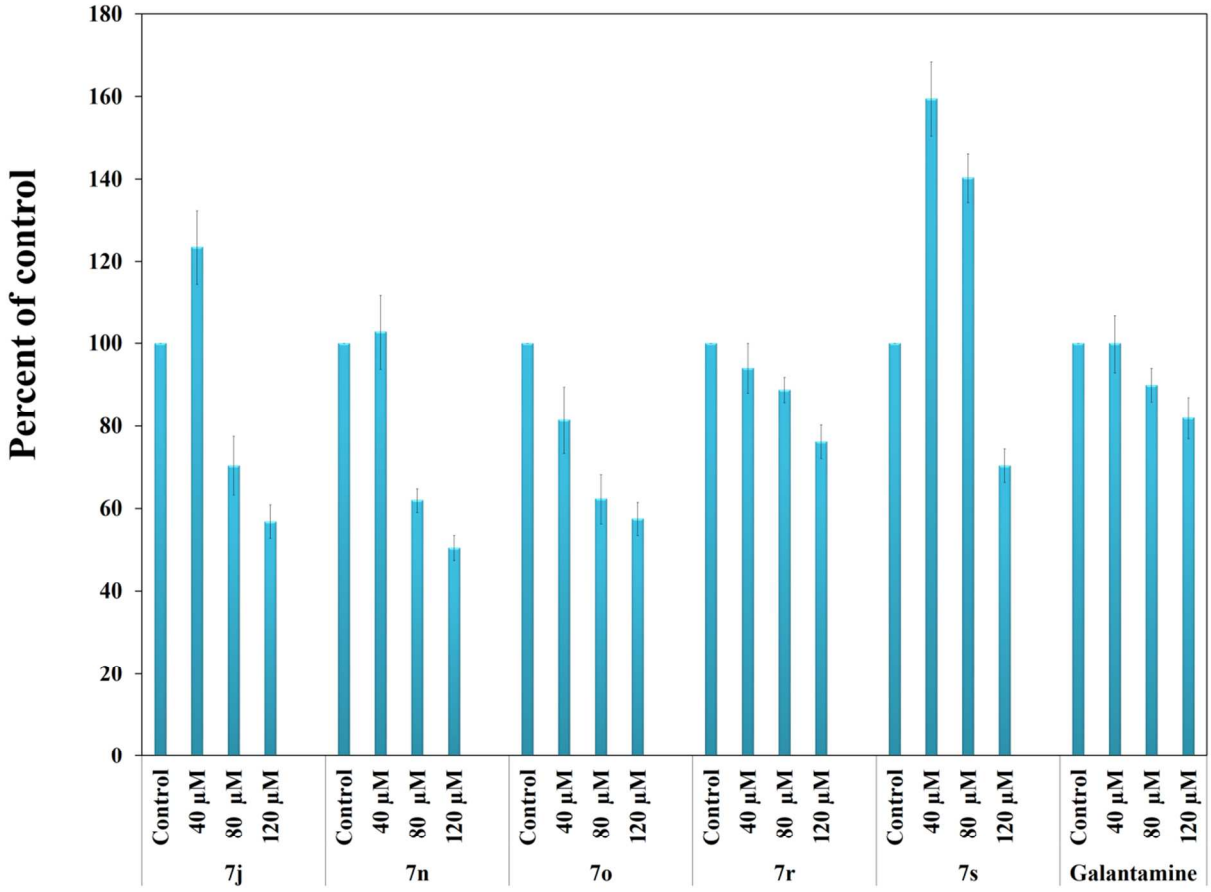
Percent of control
180
160
140
120
100
80
60
40
20
0
Control
40 µM
80 µM
120 µM
7j
7n
7o
7r
7s
Galantamine

Figure 4.

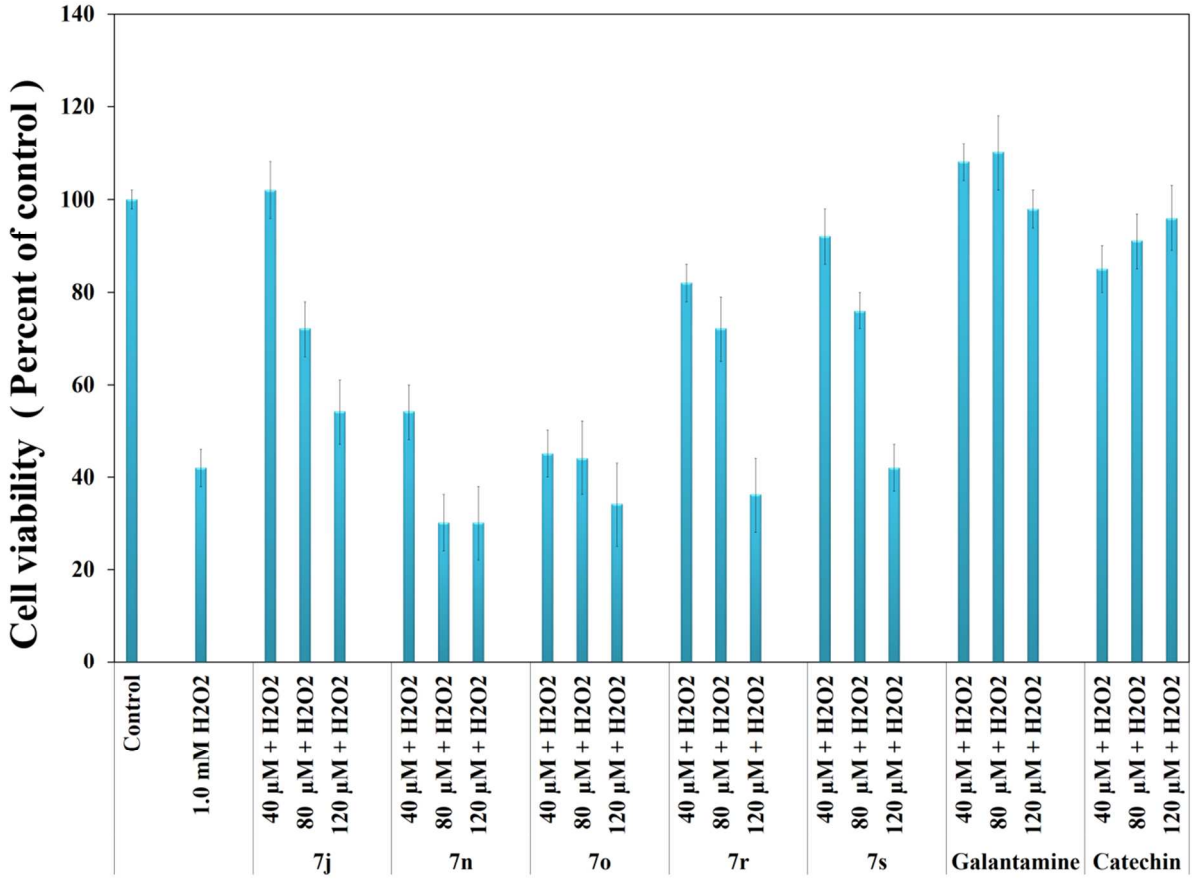
Cell viability (Percent of control)
140
120
100
80
60
40
20
0
Control
1.0 mM H2O2
40 µM + H2O2
80 µM + H2O2
120 µM + H2O2
7j
7n
7o
7r
7s
Galantamine
Catechin

Figure 5.

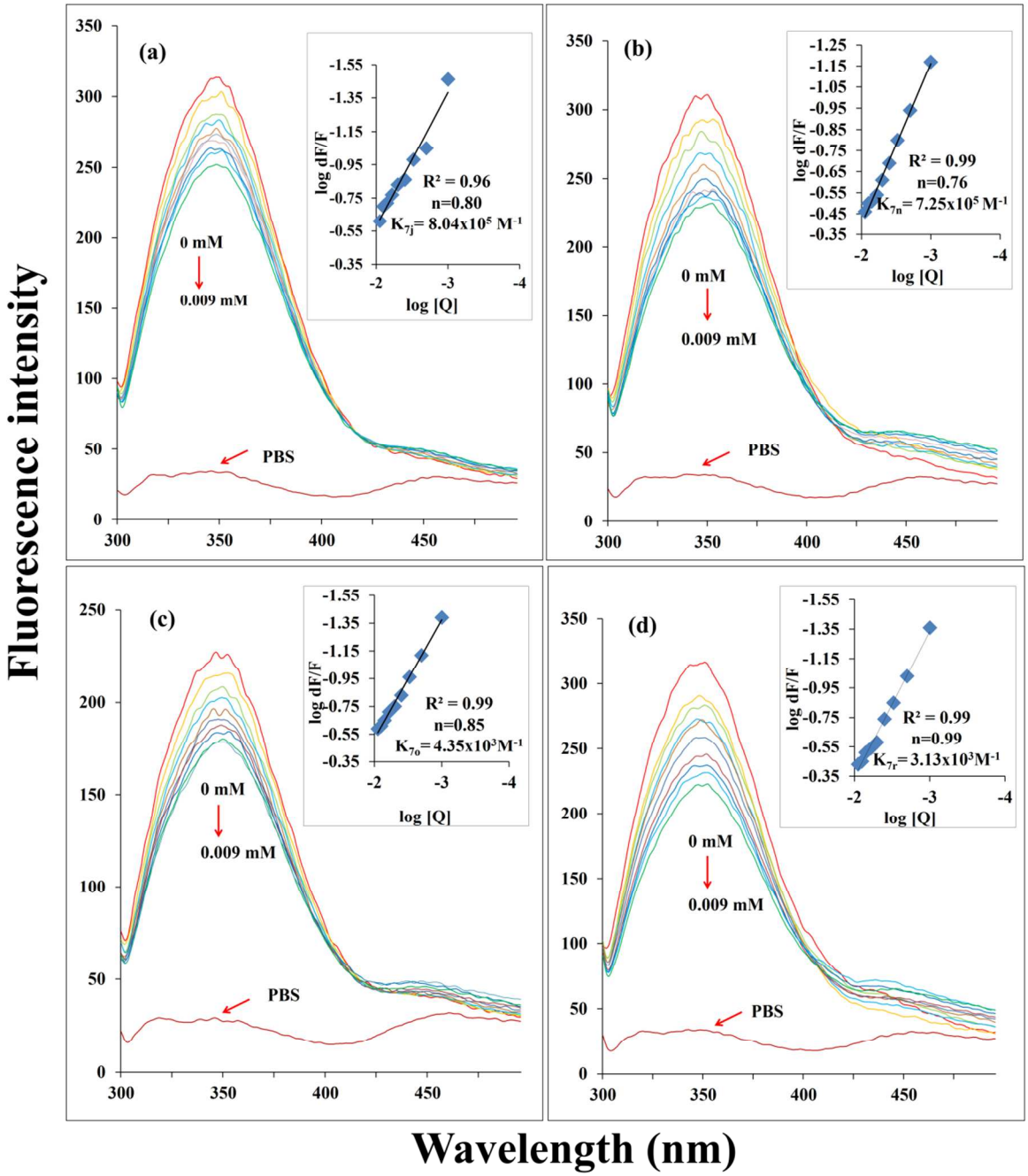
Fluorescence intensity
Wavelength (nm)
(a)
0 mM
0.009 mM
PBS
log dF/F
log [Q]
R² = 0.96
n=0.80
K7j= 8.04x10⁵ M⁻¹
(b)
R² = 0.99
n=0.76
K7n= 7.25x10⁵ M⁻¹
(c)
R² = 0.99
n=0.85
K7o= 4.35x10³M⁻¹
(d)
R² = 0.99
n=0.99
K7r= 3.13x10³M⁻¹

Figure 6.

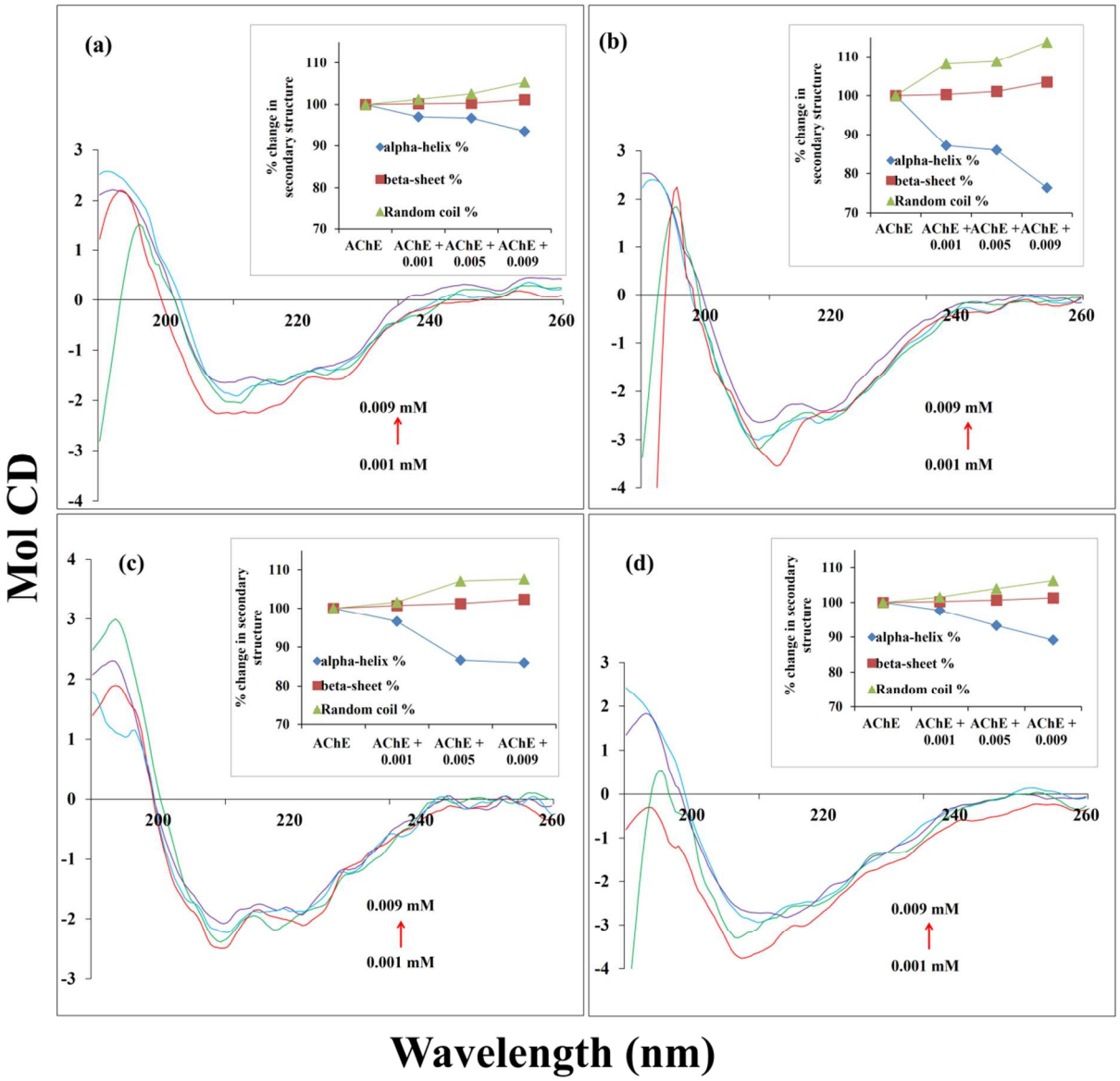
(a)
(b)
(c)
(d)
% change in secondary structure
alpha-helix %
beta-sheet %
Random coil %
AChE
AChE + 0.001
AChE + 0.005
AChE + 0.009
0.009 mM
0.001 mM
Mol CD
Wavelength (nm)

Figure 7.

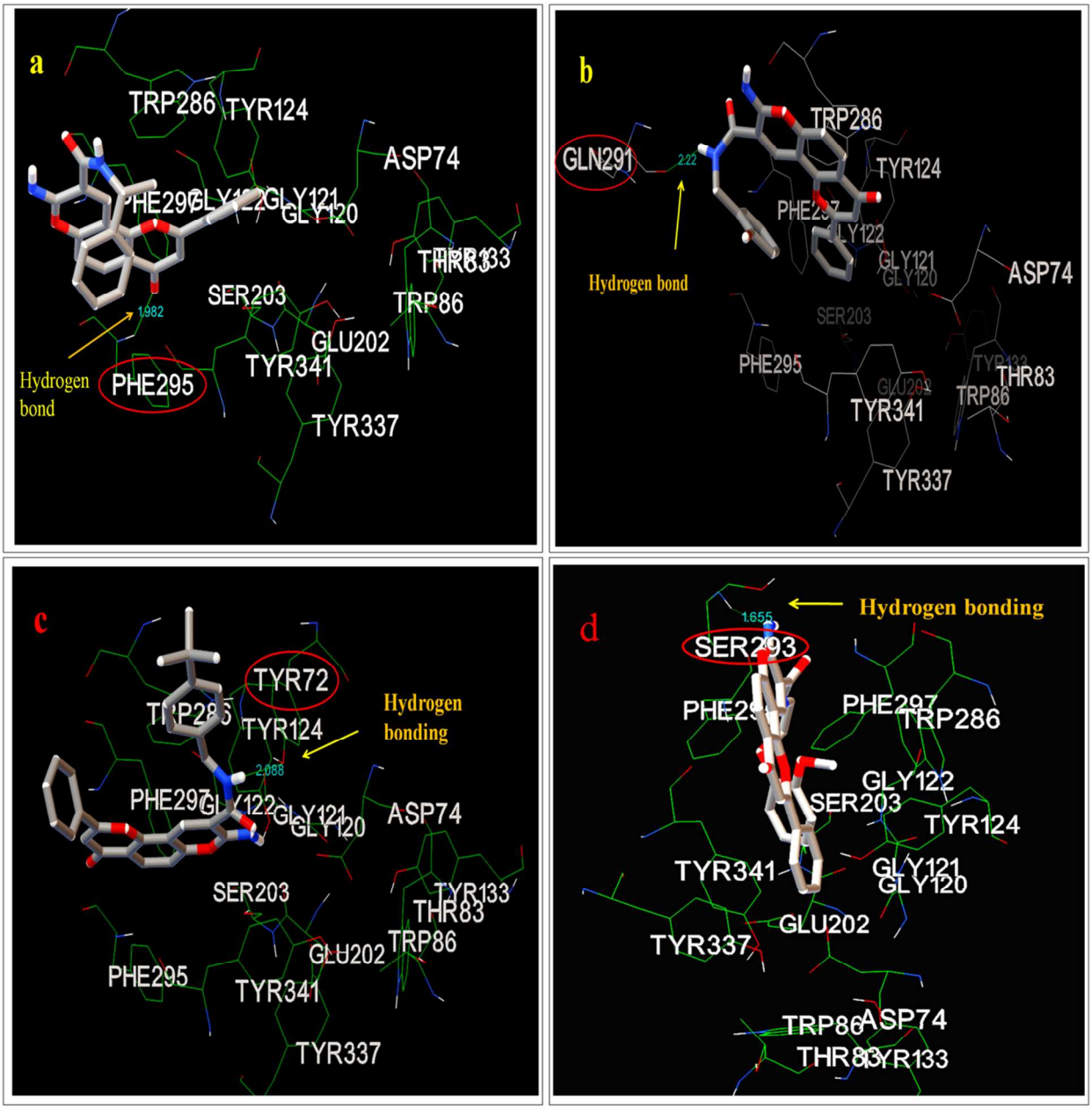
a
TRP286
TYR124
ASP74
PHE297
GLY122
GLY121
GLY120
THR83
SER203
TRP86
1.982
GLU202
TYR341
Hydrogen bond
PHE295
TYR337
b
GLN291
2.22
TRP286
TYR124
Hydrogen bond
GLY121
GLY120
ASP74
SER203
PHE295
THR83
TRP86
TYR341
TYR337
c
TYR72
TYR124
Hydrogen bonding
2.088
PHE297
GLY121
GLY120
ASP74
SER203
TYR133
THR83
TRP86
GLU202
PHE295
TYR341
TYR337
d
1.655
Hydrogen bonding
SER203
PHE297
TRP286
GLY122
SER203
TYR124
TYR341
GLY121
GLY120
GLU202
TYR337
TRP86
ASP74
THR83
TYR133

Figure 8.

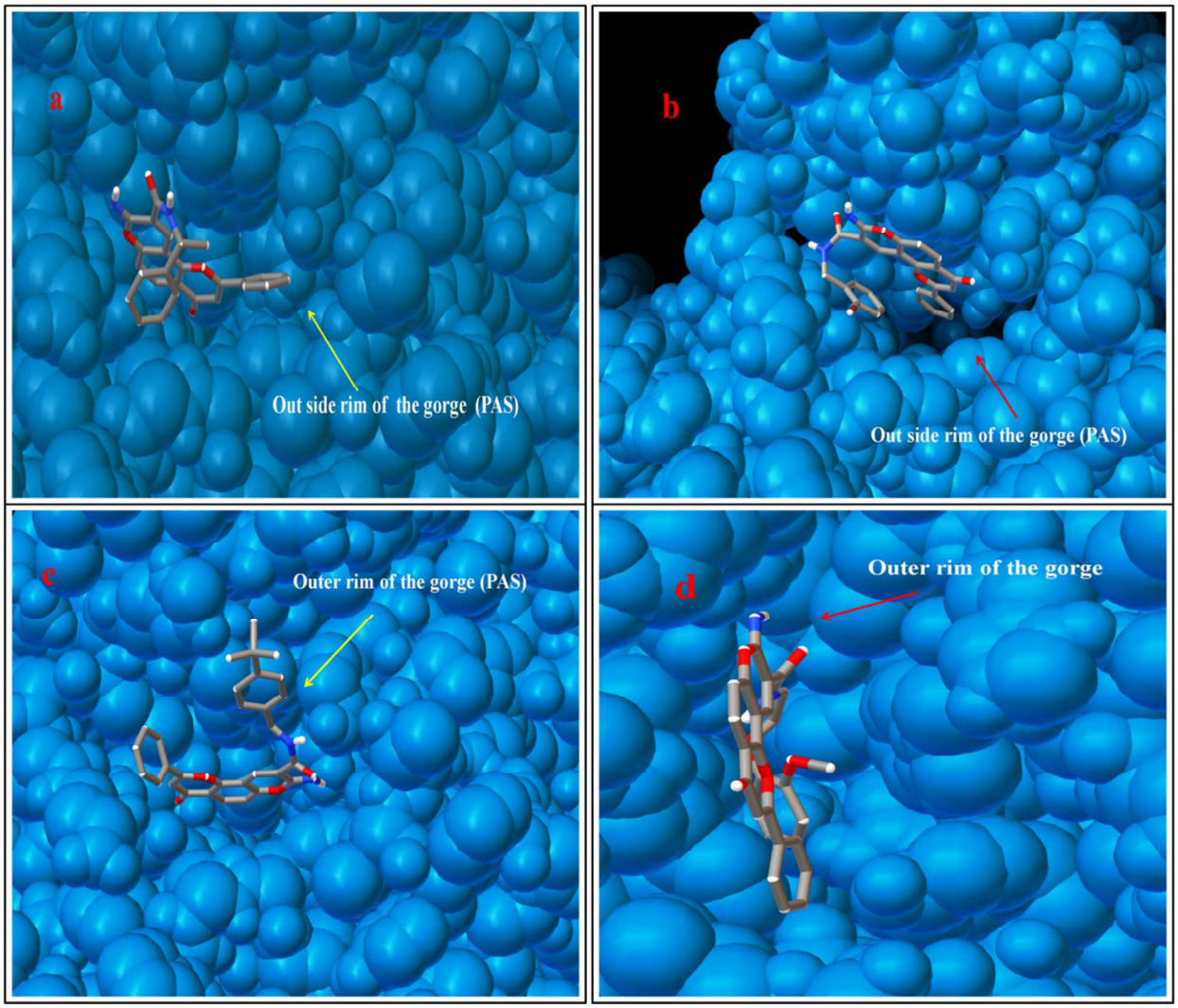
a
Out side rim of the gorge (PAS)
b
Out side rim of the gorge (PAS)
c
Outer rim of the gorge (PAS)
d
Outer rim of the gorge

Table of Contents Graphics

Flavone-cyanoacetamide hybrids as multifunctional agents for Alzheimer's disease and unraveling their mechanism of action with acetylcholinesterase

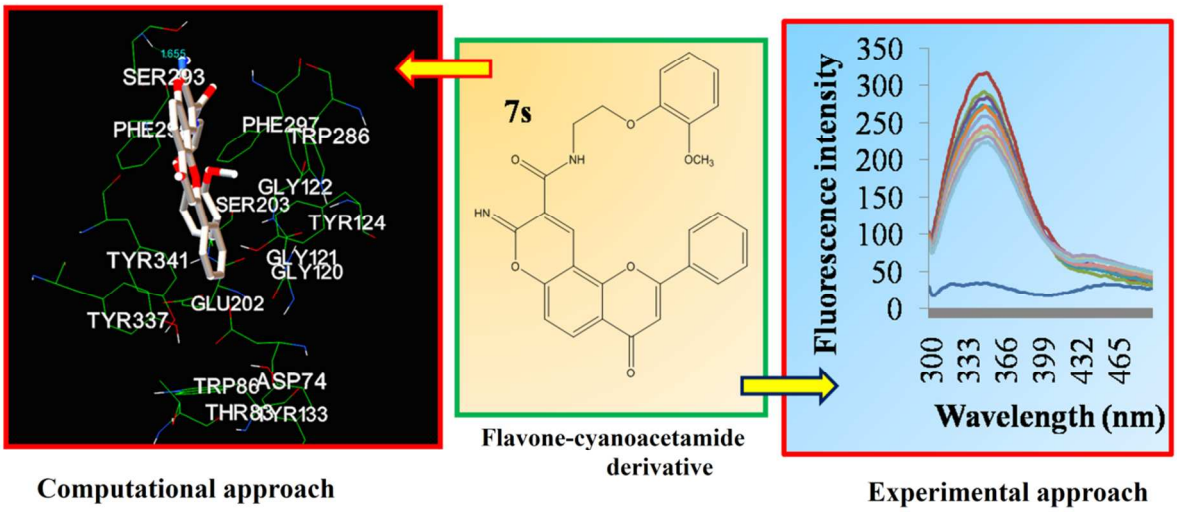

Computational approach

Flavone-cyanoacetamide derivative

Experimental approach